C-mip Impairs Podocyte Proximal Signaling

And Induces Heavy Proteinuria

Shao-yu Zhang,[1,2] Maud Kamal,[1,2] Karine Dahan,[1,2] André Pawlak,[1,2] Virginie Ory,[1,2] Dominique Desvaux,[1,2] Vincent Audard,[1,2] Marina Candelier,[1,2] Fatima Ben Mohamed,[1,2] Marie Matignon,[1,2] Christo Christov,[3,4] Xavier Decrouy,[4] Veronique Bernard,[5] Gilles Mangiapan,[6] Philippe Lang,[1,2,7,8] Georges Guellaën,[1,2] Pierre Ronco[9,10,11] and Djillali Sahali[1,2,7, 8*]

[1] INSERM, UMR 955, Equipe 21, Créteil, F-94010, France;

[2] Université Paris-Est Créteil Val-de-Marne, UMRS 955, Equipe 21, Créteil, F-94010, France;

[3] AP-HP, Groupe hospitalier Henri Mondor - Albert Chenevier, Service d'histologie, Département de Pathologie, Créteil, F-94010, France;

[4] INSERM, UMR 955, Plate-Forme d'Imagerie Cellulaire et Tissulaire, Créteil, F-94010, France ;

[5] INSERM, UMR 952, CNRS UMR7224, Université Pierre et Marie Curie, Paris, France ;

[6] Centre hospitalier intercommunal, Service de pneumologie, Créteil, F-94010, France;

[7] AP-HP, Groupe hospitalier Henri Mondor - Albert Chenevier, Service de Néphrologie, Créteil, F-94010 France ;

[8] Institut francilien de recherche en néphrologie et transplantation ;

[9] INSERM UMRS-702, Paris, F75020, France ;

[10] UPMC Univ-Paris 6; Paris 75252 Cedex 05, France

[11] AP-HP, Hôpital Tenon, Service de Néphrologie et Dialyses, Paris, F-75020, France.

MK, KD and AP contributed equally to this work

The authors have declared that no conflict of interest exists

* To whom correspondence should be addressed. Telephone: 33149812537. Fax: 33149812539 ;

E-mail: dil.sahali@inserm.fr.

Abstract

Idiopathic nephrotic syndrome comprises several podocyte diseases of unknown origin, affecting the glomerular podocyte, which plays a key role in controlling the permeability of the kidney filter to proteins. It is characterized by the daily loss of more than 3 g of protein in urine, with no inflammatory lesions or cell infiltration. Nephrotic syndrome may be associated with serious complications, including sodium retention, hyperlipidemia, infectious diseases and thromboembolic events. The molecular mechanisms underlying non genetic nephrotic syndromes are unknown. We report here that the abundance of c-mip (c-maf inducing protein) increases in the podocytes of patients with acquired idiopathic nephrotic syndromes, including minimal change nephrotic syndrome (MCNS), a subset of focal and segmental glomerulosclerosis (FSGS) and membranous nephropathy (MN), in which the podocyte is the main target of injury. Transgenic mice overproducing c-mip in podocytes developed proteinuria without morphological alterations, inflammatory lesions or cell infiltration. We found that c-mip turned off podocyte signaling by preventing the interaction of nephrin with the tyrosine kinase Fyn, thereby decreasing nephrin phosphorylation *in vitro* and *in vivo*. Moreover, c-mip inhibited interactions between Fyn and N-WASP and between Nck and nephrin, potentially accounting for cytoskeletal disorganization and the effacement of foot processes. The intravenous injection of a small interfering RNA (siRNA) targeting c-mip prevented lipopolysaccharide-induced proteinuria in mice. These results provide new insights into the molecular mechanism of acquired podocyte diseases.

Introduction

The kidney filters 180 liters of plasma daily, through the glomerular filtration barrier, a highly specialized glomerular structure consisting of a fenestrated endothelial cell layer, a glomerular basement membrane (GBM), and a layer of epithelial cells called podocytes, wich cover the external side of the glomerular capillary loop *(1)*. The podocyte is a terminally differentiated epithelial cell immersed in the urinary space and anchored to the underlying GBM by large cell expansions, known as foot processes *(2)*. The slit diaphragm is a 40 nm junction structure that links the interdigitating foot processes from neighboring podocytes *(2)*. The glomerular filtrate passes first through the fenestrated endothelium, then through the GBM, and finally through the slit diaphragm, which serves as the principal size-selective macromolecular filter, preventing the passage of large proteins into the urinary space *(2)*. The effacement of foot processes is a common ultrastructural feature of nephrotic syndrome (defined by massive urinary protein loss), regardless of its etiology *(3)*. It may result from structural or functional changes in the subcellular compartments of the podocyte, including the cytoskeleton, slit diaphragm, GBM interface, and apical domains *(4)*. The molecular mechanisms underlying these alterations remained elusive until the identification of mutations associated with familial forms of steroid-resistant nephrotic syndrome. These mutations were identified in genes encoding nephrin (NPHS1), a transmembrane protein that functions as an adhesion molecule, podocin (NPHS2), a lipid raft-associated protein, CD2-associated protein (CD2-AP), an adapter protein, the cytoskeletal protein α-actinin4, the transient receptor potential channel 6 (TRPC6) and phospholipase Cε, a regulator of activated G protein signals *(5-10)*.

In addition to playing a structural role in the slit diaphragm, nephrin is a signaling molecule involved in several intracellular pathways within podocytes *(11)*. The clustering of nephrin in lipid rafts as demonstrated by antibody crosslinking induces activation of the Src-family kinase Fyn, which binds to and phosphorylates the cytoplasmic domain of nephrin. The

phosphorylated nephrin interacts with podocin, CD2-AP and the p85 subunit of phosphoinositide-3 kinase (PI3K), thereby activating the Akt signaling pathway *(12-14)*. Nephrin phosphorylation promotes the sequential recruitment of Nck and activated Wiskott-Aldrich syndrome protein (WASP) to lipid rafts. The Nck subfamily of adaptor proteins has two members, Nck1 and Nck2, each containing three N-terminal SH3 domains and a single C-terminal SH2 domain *(13)*. The SH3 domain of Nck interacts with N-WASP, whereas the SH2 domain binds to the cytoplasmic domain of nephrin *(13)*. N-WASP, a member of the WASP family proteins, is a potent inducer of Arp2/3-mediated actin polymerization *(15)*. The Nck adaptor protein activates N-WASP and promotes cytoskeletal rearrangement (*13*). Within lipid rafts, Fyn interacts with and phosphorylates N-WASP *(13, 16)*. The interaction of Fyn with CD2-AP and synaptopodin links nephrin-mediated proximal signaling to the actin cytoskeleton *(17)*. The slit diaphragm thus acts as a signaling platform on which multiple signals converge *(4)*.

We carried out subtractive and differential screening of mRNA abundance in the T-cells of MCNS patients experiencing a relapse. We identified *c-mip* (c-maf inducing protein), a gene encoding an 86-kDa protein, as significantly expressed in these patients *(18)*. The predicted structure of c-mip includes an N-terminal region containing a pleckstrin homology domain (PH), a central region containing docking sites for 14-3-3 protein, protein kinase C (PKC), and extracellular signal-regulated kinase (ERK), an SH3 domain similar to the p85 regulatory subunit of PI3K and a C-terminal region containing a leucine-rich repeat (LRR) domain.

We report here a high abundance of c-mip in the podocytes of patients with acquired idiopathic nephrotic syndrome, which covers three differents types of lesions of unknown origin, including MCNS, a subset of FSGS, and MN, in which the pococyte is the main target of injury. A feature common to these diseases is generalized edema resulting from massive proteinuria, hypoalbuminemia and sodium retention. These conditions may be complicated by infectious and thromboembolic events. MCNS and FSGS account for 70% and 20%, respectively, of the cases of idiopathic nephrotic syndrome in children, and of these two diseases accounts for 25% each of the cases in adults *(19-21)*. The hallmark of MCNS is an absence of inflammatory injury and

immune complex deposits in the glomeruli, whereas FSGS is characterized by the adhesion of the glomerular tuft to Bowman's capsule *(22)*. MCNS seems to be a single reasonably uniform entity combining immune and podocyte disorders, whereas FSGS appears to be a heterogeneous disease, of immune or non-immune origins *(23)*. Membranous nephropathy, which is rare in children, is characterized by the presence ofprominent immune complex deposits between the podocytes and the glomerular basement membrane *(24)*. The effacement of podocyte foot processes is a common lesion suggestive of cytoskeletal alterations.

The production of c-mip was also induced in an experimental mouse model of nephrotic proteinuria induced by LPS. Transgenic mice overproducing c-mip in the podocytes developed a nephrotic syndrome without inflammatory lesions or cell infiltrations. The c-mip protein bound Fyn directly *in vitro* and *in vivo* and prevented the interaction of Fyn with nephrin and N-WASP, thereby decreasing nephrin phosphorylation and causing cytoskeletal disorganization. The knockdown of c-mip by RNA interference (RNAi) techniques prevented the development of proteinuria in LPS-treated mice. Thus, c-mip appears to be a key player in podocyte dysfunction.

Results

c-mip is detected in the kidneys of patients with MCNS and other glomerular diseases

The pathogenesis of MCNS involves the dysfunction of lymphocytes and podocytes through an unknown mechanism *(23)*. This syndrome can be induced into remission (defined by the disappearance of proteinuria) following steroid therapy, but relapses are frequent and may require the initiation of cyclosporine treatment. Our initial studies of c-mip led us to examine whether the abundance of c-mip increased in the podocytes of patients with MCNS. We screened 15 adult patients with MCNS relapse (Table S1). In situ hybridization (ISH) with an antisense *c-mip* probe revealed a signal that was largely restricted to the podocytes; this finding was confirmed by immunohistochemical analysis with a rabbit polyclonal antibody directed against c-mip (Fig 1A). We carried out confocal microscopy analyses of kidney biopsy specimens labeled with c-mip and nephrin antibodies. We were unable to detect c-mip in normal human kidney, either in the glomeruli or in extra-glomerular structures, whereas nephrin was clearly visualized (Fig. 1B, upper panel). By contrast, in biopsy specimens from MCNS patients in relapse, c-mip was detectable and diffusely distributed along the external side of the capillary loops (Fig. 1B, lower panel). We analyzed the abundance of c-mip during remission, by carrying out immunolabeling for c-mip on kidney biopsy specimens from five MCNS patients who were steroid sensitive but were nonetheless subject to frequent relapses and therefore received an additional cyclosporine-based therapy. c-mip was scarcely detected by immunohistochemical analysis in two patients and was undetectable in the other three patients (Table S1).

We screened patients with idiopathic MN, FSGS, HIV-associated nephropathy (HIVAN), IgA nephropathy and diabetic nephropathy. All patients presented nephrotic proteinuria at the time of biopsy (Table S1). Kidney biopsy specimens from patients with primary FSGS were analyzed by both ISH (fig. S1) and immunohistochemistry (fig. S2). We detected c-mip by these methods in only four of the 10 patients studied. In these cases, the course of the disease was complicated by frequent relapses requiring

additional cyclosporine treatment**.** The distribution of c-mip was similar to that observed in MCNS biopsies but less nephrin was detected. In the other patients with FSGS in whom c-mip was not detected, the glomerular disease occurred in the context of obesity and hypertension (4 patients), sarcoidosis (1 patient) and strongyloidiasis (1 patient). These results suggest that c-mip abundance may be increased in a particular subgroup of patients with FSGS, possibly those with disease of immune origin. The abundance of c-mip was found to be high in 11 of 12 biopsies of patients with idiopathic MN (fig. S1 and fig. S2). We did not detect *c-mip* mRNA in the glomeruli of patients with nephrotic proteinuria caused by diabetic nephropathy, IgA nephropathy or HIVAN (Table S1 and fig. S1). These findings suggest that c-mip induction is not a consequence of nephrotic proteinuria.

c-mip overproduction in podocytes *in vitro* inhibits nephrin phosphorylation and causes cytoskeletal disorganization

To understand the effects of c-mip on podocyte function, we established podocyte cell lines that stably expressed a tetracycline-inducible plasmid encoding c-mip. In non induced cells, c-mip was not detectable in podocytes, which displayed a well developed actin network with stress fibers (long intracellular bundles of actin filaments) (Fig. 2A). The induction of c-mip expression by tetracycline was associated with a loss of stress fibers (Fig. 2A).

Next, we sought to determine whether these morphological alterations were associated with changes in the abundance of proteins involved in podocyte signaling. We detected c-mip 48 hours after the addition of tetracycline (Fig. 2B). The protein has a PH domain and some proteins containing this domain are recruited to lipid rafts upon activation *(25)*. Fyn, which provides the early proximal signal, is located in lipid rafts (*26*). We therefore investigated the effects of c-mip on Fyn signaling. Immunoblotting of podocyte protein lysates showed that c-mip overproduction triggered the accumulation of Fyn molecules phosphorylated at the Tyr^{528} residue ($pTyr^{528}$-Fyn), suggesting that c-mip prevents Fyn activation (Fig. 2B). Consequently, the amount of phosphorylated nephrin (p-nephrin) was reduced upon induction of c-mip, although the total abundance of nephrin appeared unaltered (Fig. 2B). The induction of c-mip was also associated with a decrease in the phosphorylation of the Ser^{473} residue of

Akt (pSer^{473}-Akt) (Fig. 2B). On the other hand, c-mip did not affect the protein abundance of CD2-AP and podocin (Fig. 2B). Taken together, these results suggest that c-mip interferes with proximal signals, inhibits nephrin activation and promotes actin cytoskeleton disorganization.

c-mip transgenic mice develop nephrotic proteinuria without inflammatory lesions or cell infiltration

To analyze the functional consequences of c-mip upregulation *in vivo*, we used a targeting system in which a single copy of the transgene was inserted into the *X-linked hypoxanthine phosphoribosyltransferase 1 hypoxanthine phosphoribosyltransferase* (*Hprt)* locus by homologous recombination (fig. S3). A cDNA containing the coding sequence of *c-mip* was inserted under the control of the nephrin promoter to drive *c-mip* expression in podocytes. The founders were crossed with wild-type C57Bl/6 and back-crossed repeatedly to obtain a homogeneous C57BL/6 genetic background. All the mice analyzed here were hemizygous males [Tg(+)] from the F4 to F10 generations. Proteinuria and urinary creatinine concentrations were determined in 294 adult Tg(+) mice from the F4 (n=109 mice), F6 (n=55 mice), F7 (n=70 mice) and F8-F10 (n=60 mice) generations. Tg(+) mice developed nephrotic proteinuria with a strong predominance of albumin (Fig. 3, A and B). Light microscopy analysis of periodic acid-Schiff (PAS) reagent-stained-kidney sections from eight-week-old proteinuric Tg(+) mice showed that glomeruli exhibited a normal architecture with little or no mesangial hypercellularity (fig. S4). Renal function was preserved as shown by the plasma creatinine concentrations measured at 3 and 6 months (fig. S4). The tubular structures and interstitium displayed no pathological changes, but some tubules were filled with protein (fig. S5, upper panel). W detected c-mip in the peripheral capillary loops of proteinuric mice, whereas it was undetectable in wild-type mice (fig. S5, middle panel). No immunoglobulin or complement deposits were observed on immunofluorescence analysis (fig. S5, lower panel). We did not detect c-mip either in tubular structures or in the interstitium. Pathological examinations of other organs did not reveal any common alterations and no abnormal mortality was noted during the observation period.

We assessed the amount of c-mip protein in MCNS and Tg(+) glomeruli, by incubating tissue sections with an anti-c-mip antibody, followed by an FITC-conjugated secondary antibody, and examining three-dimensional images throughout the entire thickness of the glomeruli (20 images per glomerulus), by confocal microscopy. We quantified the fluorescence of the most representative slice from the image stack. Given the differences in size between the glomeruli of mice and humans, precluding direct comparison, we quantified the site-specific fluorescent labeling lining the capillary loop, and normalized the value obtained by dividing it by total glomerular area, for each glomerulus (table S2 and fig. S6).

Electron microscopy analysis of glomeruli in Tg(+) mice revealed the effacement of foot processes with flattened podocytes (as usually observed in patients with nephrotic proteinuria), whereas wild-type mice had normal foot processes (Fig. 3, C and D). Slit diaphragms appeared narrow in most glomeruli and were absent in some areas, with the formation of occluding junctions between neighboring foot processes. These features were not observed in normal littermates. The podocyte foot processes were significantly wider in Tg(+) than in wild-type mice (Fig. 3E). The glomerular basement membrane (GBM) appeared normal. The tubules and interstitium were normal. Immunogold labeling revealed that c-mip was predominantly, but not exclusively located in the major and secondary foot processes close to the slit diaphragm (fig. S4).

We followed the course of glomerular disease in Tg(+) mice, from birth until the age of one year. Semi-quantitative determinations of urinary protein levels were carried out with a dipstick in newborn mice of the F7 generation (table S3). Proteinuria was detected in 70% of five day-old mice and in 79% of three-old mice. Electron microscopy studies showed numerous areas of foot process effacement and foot processes with an abnormal morphology (fig. S7). We then determined urinary protein concentrations in four groups of mice, at various ages, from one to 12 months (fig. S8A). Based on these concentrations, it was clear that glomerular disease was established in these mice by the age of one to three months. Histological analyses of kidney sections, including 30 to 50 glomeruli per mouse were carried out blind, and scores were determined for ten mice for each age group. At three months of age, glomeruli of proteinuric Tg(+) mice exhibited a normal morphology (fig. S8B). At six months of age, 25% of glomeruli showed mesangial hypercellularity. At one-year of age, approximately 25% of the glomeruli

displayed a clear expansion of the mesangial matrix and some FSGS-like lesions, as observed in some patients with MCNS who will develop FSGS. We found no correlation between the protein concentration in urine and the extent of the mesangial changes.

The podocytes of c-mip transgenic mice have an abnormal phenotype

We performed confocal microscopy analysis for various markers of mature podocytes. Nephrin and phosphorylated nephrin exhibited a continuous linear distribution along the peripheral capillary loop in wild-type mice. In Tg(+) glomeruli, the abundance of nephrin was less abundant at the podocyte membrane, where granular staining was observed and lower amounts of nephrin phosphorylation were detected (fig. S9). Our *in vitro* studies suggested that c-mip interfered with podocyte proximal activation (Fig. 2B). Consistent with these findings, eight-and ten-week-old Tg(+) mice had less phosphorylated nephrin than their wild-type littermates, although the total abundance of nephrin was unchanged (Fig. 4A). These alterations were associated with an increase in the abundance of the inactive forms of Fyn (pTyr^{528}-Fyn) and Akt (Fig. 4B). No c-mip was detected in wild-type mice, suggesting that the abundance of c-mip may be kept low under normal conditions. The inactivation of Akt was confirmed by immunofluorescence analyses of kidney sections. The pSer^{473}-Akt form was visualized along the peripheral capillary loop at the site of the podocytes in wild-type mice but was not detected in Tg(+) mice (Fig. 4C). The amount of pSer^{473}-Akt was also significantly lower in the kidneys of patients with MCNS than in those of patients with IgA nephropathy or diabetic nephropathy (Fig. 4C and fig. S10), highlighting the pathophysiological relevance of this mouse model to the human disease.

c-mip binds Fyn and inhibits the interactions of Fyn with nephrin and N-WASP

Because Akt was inactive in glomeruli from MCNS biopsies and in c-mip Tg mice, and as c-mip decreased the amount of nephrin phosphorylation *in vitro*, we investigated whether c-mip interfered with Fyn-mediated proximal signaling. In a preliminary analysis, c-mip protein was not detected in human embryonic kidney (HEK) cells (fig. S11A). In coimmunoprecipitation experiments with protein lysates from transfected HEK cells, c-mip bound Fyn (fig. S12A, upper panel). Endogenous Fyn was also

immunoprecipitated with c-mip (fig. S12A, upper panel). This interaction seemed to be direct because purified recombinant c-mip was immunoprecipitated with recombinant Fyn (fig. S12A, middle panel). Coimmunoprecipitation analysis with deletion mutants of c-mip revealed that c-mip interacted with Fyn through its PH domain (fig. S12A, lower panel).

We next coexpressed c-mip, nephrin and Fyn (to mimic biochemical events seen in nephrotic syndromes) and determined whether nephrin retained its ability to interact with Fyn. Coimmunoprecipitation experiments showed that c-mip prevented the interaction of nephrin with Fyn (fig. S12B, upper panel). We then investigated whether the inability of nephrin to interact with Fyn influenced its phosphorylation status. Coexpression of nephrin and Fyn induced the phosphorylation of nephrin at residue Tyr^{1208}; this phosphorylation event was prevented by coexpression of c-mip (fig. S12B, lower panel).

Activated Fyn binds and phosphorylates N-WASP *(13, 16)*, facilitating the anchoring of the cytoskeleton to lipid rafts (*27*). Immunoprecipitation experiments with protein lysates from transfected HEK cells indicated that Fyn bound to N-WASP but that this interaction was blocked in the presence of c-mip (fig. S12C). We found that c-mip was coimmunoprecipitated with Fyn from glomerular extracts from Tg(+) mice, but not those from wild-type mice (Fig. 5A). The amount of nephrin immunoprecipitated with Fyn in Tg(+) mice was lower than in wild-type mice (Fig. 5B). Moreover, Tg(+) mice displayed lower amounts of nephrin phosphorylation, even though the amounts of nephrin immunoprecipitated in wild-type and Tg(+) mice were comparable (Fig. 4A). Nck binds N-WASP through its SH3 domain and nephrin through its SH2 domain *(12, 13, 16)*. The interactions of Fyn with N-WASP (Fig. 5C) and Nck with nephrin (Fig. 5, D and E) were weaker in the presence of c-mip. Together, these results suggest that c-mip interacts with Fyn and alters proximal signaling and cytoskeleton reorganization by disrupting the interactions of Fyn with N-WASP and nephrin, respectively.

RNAi directed against c-mip prevents induction of proteinuria in LPS-treated mice

To determine whether the silencing of endogenous c-mip could prevent the development of proteinuria, we took advantage of our observations that the increase in c-mip abundance in LPS-treated mice occurred at the same time as the induction of proteinuria (Fig. 6A). In this model, we confirmed that c-mip was

present in podocyte foot processes and that it bound Fyn (Fig. 6A). We detected c-mip mostly in flattened podocytes, rather than in podocytes with normal foot processes (fig. S13). No c-mip was detected in splenocytes from LPS-treated mice. However, we nevertheless investigated whether the induction of c-mip in podocytes from LPS-treated mice required T-cell activation. In SCID mice, which lack both cellular and humoral immunity, LPS injection induced significant proteinuria and an increase in c-mip abundance in podocytes (Fig. 6B).

We used RNA interference to knock down c-mip in vivo. We injected fluorescently labeled c-mip siRNA (10 mg/kg) into the internal jugular vein and then, 30 min later, we injected LPS (200 μg in PBS) into the peritoneum. Proteinuria was decreased by 70% in LPS-treated mice injected with siRNA (Fig. 6C), compared to those injected with LPS alone (urinary protein/creatinine ratio, 4.52 ± 1.75 compared to 19.51 ±1.35, respectively). The transfection reagent (Invivofectamine) slightly increased the proteinuria above the values observed for non-injected wild type mice (6.5 ± 1.41 compared to 2.25 ± 0.9, respectively), an effect that may be due to its cationic structure. Confocal immunofluorescence analysis showed that c-mip siRNA was efficiently delivered to podocytes (Fig. 6C). The abundance of c-mip in podocytes was lower in mice injected with c-mip siRNA and LPS, and increased in mice receiving LPS alone (Fig. 6C). The amount of nephrin and phosphorylated nephrin appeared to be reduced in many glomeruli of LPS-treated mice, as compared with mice treated with both siRNA and LPS (Fig. 7A). The amount of phosphorylated Akt (pSer^{473}-Akt) was significantly reduced in LPS mice, whereas no significant difference was observed between siRNA-LPS and normal mice (Fig. 7B). These results suggest that it may be possible to prevent proximal signaling disorders and the development of proteinuria by inhibiting increases in the abundance of c-mip.

Discussion

The molecular pathogenesis of the most common acquired glomerular diseases associated with nephrotic syndrome remains to be elucidated. In this study, we provide evidence that: (i) the abundance of c-mip is selectively increased in the podocytes of patients with MCNS during relapse and decreased during remission; (ii) c-mip is detected in only a few patients with FSGS, confirming the heterogeneous nature of this entity, and in most patients with MN but not in other diseases with proteinuria in the nephrotic range analyzed to date; (iii) the overeproduction of c-mip in the podocytes of transgenic mice induces heavy proteinuria with podocyte foot process effacement, but without inflammatory lesions and immune complex deposits; (iv) c-mip binds Fyn *in vivo* and prevents the phosphorylation of nephrin and the recruitment of N-WASP and Nck, thus disturbing downstream signaling events, ultimately resulting in cytoskeleton disorganization and protein leakage; (v) the silencing of endogenous c-mip by RNAi prevents the induction of proteinuria in LPS-treated mice.

The higher abundance of c-mip in the podocytes of patients with MN, a glomerular disease characterized by subepithelial immune complex deposits, was unexpected. Like patients with MCNS, massive proteinuria in MN occurs in the absence of inflammatory cells *(24)*. In both experimental and human MN, immune complexes forming electron-dense deposits lead to complement activation and generation of the C5b-9/Mac complex, which in turn, induces alterations in the podocyte membrane and slit diaphragm, resulting in proteinuria *(28)*. However, there are several lines of evidence to suggest that the mechanisms underlying the induction of proteinuria may be more complex. First, the remission of nephrotic syndrome may be observed in patients with MN, despite the persistence of electron-dense deposits *(29)*, which suggests that additional mechanisms may be required to alter slit diaphragm signaling. Second, active and passive Heymann nephritis can be induced in rats lacking complement component C6 and incapable of forming C5b-9 (also known as Mac) *(30, 31)*, suggesting that the local activation of complement is not required for proteinuria induction. Third, the transplantation of kidneys from rats with Heymann nephritis, an experimental rat model of MN, into syngeneic hosts induces the

clearing of subepithelial immune deposits with no decrease in proteinuria *(32)*. Fourth, both MCNS and MN podocytopathies are associated with a decrease in nephrin abundance and changes in the distribution of nephrin *(33)*, as observed in our c-mip transgenic mice. The injuries initiating the nephrotic syndrome differ in these two diseases targeting podocytes, but our results suggest that the underlying mechanisms may have signaling pathways in common and should be reconsidered in the light of our findings concerning c-mip induction.

T lymphocytes and podocytes constitutively produce several proteins such as CD2-AP, Fyn, and Nck, that play a key role in signaling and cytoskeleton reorganization in both these cell types. Mutations or experimental ablations of the genes encoding CD2-AP and Fyn are associated with glomerular filtration defects and immune disorders, respectively *(34, 35)*. By contrast, c-mip is, to our knowledge, the first gene, shown to be quiescent under basal conditions but induced in both cell types in pathological situations, thus forming a bridge between immune alterations and podocyte dysfunction.

Tg mice expressing c-mip specifically in podocytes under the control of the nephrin promoter develop a glomerular disease characterized by heavy proteinuria with a predominance of albumin, diffuse effacement of foot processes and an absence of immune deposits. The similarities between kidney biopsy findings for patients with podocyte diseases and c-mip Tg mice suggests that mice constitute a suitable model suitable for investigations of the mechanisms underlying nephrotic proteinuria.

We have deciphered the molecular mechanisms downstream from c-mip induction that lead to changes in signaling at the slit diaphragm, resulting in cytoskeletal disorganization and protein leakage through the glomerular capillary wall. Our studies, in stably transfected podocyte cell lines with inducible c-mip expression and a transgenic mouse model, provide support for a critical inhibitory role of c-mip in podocyte proximal signaling. Fyn was mostly detected in an inactive form in podocytes overexpressing *c-mip in vitro* and *in vivo*, consistent with a blockade of proximal signaling. We provide evidence that c-mip binds Fyn and prevents the interaction of nephrin with Fyn, thereby decreasing nephrin phosphorylation. The inability of Fyn to phosphorylate nephrin may facilitate the interaction of nephrin with β-arrestin2 and its subsequent endocytosis and degradation *(36)*. In agreement with our *in vitro* data, nephrin phosphorylation abundance was found lower in the podocytes of adult Tg(+) mice that in those of

wild-type mice. The phosphorylation of Akt was consistently lower in the glomeruli of patients with MCNS, but increased in those of patients with diabetic nephropathy, except in areas of glomerulosclerosis.

Nephrin phosphorylation promotes the recruitment of Nck and subsequent interactions of Fyn with N-WASP in lipid rafts. Thus, decrease in nephrin phosphorylation disrupts the interactions of this protein with Nck and N-WASP. These alterations hamper nephrin signaling and lead to cytoskeletal disorganization, a key event in the induction of proteinuria *(13, 37)*. These data suggest that c-mip dissociates Fyn-mediated early podocyte proximal signals from cytoskeletal organization in podocytes.

LPS induces podocyte foot process effacement *(38)* and decreases the abundance of *nephrin* mRNA *(39)*. We show here that many glomeruli in LPS mice display a segmental loss of nephrin and phosphorylated nephrin, and lower amounts of Akt phosphorylation. These phenotypes were not observed in mice injected with c-mip siRNA. These results suggest that the increase in c-mip abundance in podocytes is sufficient to induce nephrotic syndrome, providing support for the hypothesis that c-mip inhibits proximal signaling. In addition to podocytes, LPS affects other cell compartments, including endothelial and tubular cells, but several findings suggest that the decrease in proteinuria results from a specific effect of c-mip siRNA on podocytes. First, genome-wide expression studies of glomerular mRNA from LPS-treated and control mice, combined with immunohistochemistry, have shown that LPS predominantly affects podocytes and their actin cytoskeleton *(39)*. Indeed, LPS induces the downregulation of many podocyte genes, including α-actinin-4, nephrin, podocin, synaptopodin and Fyn *(39)*. LPS-induced proteinuria in SCID mice is correlated with an increase in the abundance of c-mip in podocytes, in the absence of T or B cell infiltration of the kidney and patent tubular or interstitial lesions.

Finally, the fact that transgenic mice expressing c-mip develop nephrotic syndrome, whereas silencing of endogenous c-mip prevents its development in LPS-treated mice suggests that c-mip plays an essential role in this disorder and identifies this protein as a potential key target for the development of new treatments.

Materials and Methods

Patients

The cohort of adult patients analyzed in this study was from our clinical department. The characteristics of these patients are summarized in Table S1. All adult patients with MCNS relapse had proteinuria levels exceeding 3 g per 24 h and severe hypoalbuminemia at the time of blood sampling, which was performed before steroid treatment. The diagnosis of kidney disease was confirmed by renal biopsy. MCNS and MN were clinically classified as idiopathic in all cases.

The control cohort included adult patients with glomerular diseases with proteinuria in the nephrotic range. Normal renal samples were supplied by the hospital tissue bank (biological resource platform, Hôpital Henri Mondor). They were obtained from patients undergoing nephrectomy for a polar kidney tumor.

Immunohistochemistry and confocal microscopy

In situ hybridization (ISH) was performed as described elsewhere *(40)*. For immunofluorescence analyses, podocytes were cultured on Lab-Tek slides (Nalge Nunc, Rochester, New York) at a subconfluent density, then fixed by incubation with 2% paraformaldehyde and 4% sucrose in phosphate-buffered saline (PBS) for 10 min at room temperature. Cells were permeabilized by incubation with 0.3% Triton X-100 for 10 min, and blocked by incubation in 1% bovine serum albumin (BSA) for 30 min. The slides were incubated overnight at 4°C with the indicated antibodies. They were then washed and incubated with the appropriate secondary biotinylated antibody (Vector Laboratories) for 10 min at room temperature, followed by a fluorescein-avidin DCS (Vector Laboratories). F-actin was visualized by incubation with FITC-conjugated phalloidin (Molecular Probes, Eugene, OR, USA). The slides were covered with Vectashield mounting medium containing DAPI, and viewed with a fluorescence microscope (Zeiss, Germany) using blue and green filters.

Immunohistochemistry studies on kidney sections were performed as described elsewhere *(40)*. Immunofluorescence studies on kidney tissues were performed on 4 μm cryostat sections fixed in acetone for 10 min, air-dried for 30 min at room temperature, then incubated in PBS for 3 min and blocked with 1% BSA in PBS. The sections were incubated with the indicated antibodies for one hour at room temperature, washed with PBS and incubated with FITC or Texas red-conjugated secondary antibodies. For dual fluorochrome labeling, the slides were simultaneously incubated with rabbit anti-cmip antibody and mouse anti-synaptopodin antibody. The slides were then washed with PBS and simultaneously incubated with FITC-conjugated goat anti-rabbit IgG and cyanine 3-conjugated sheep anti-mouse IgG. Sections were examined by fluorescence microscopy (Zeiss). The relative amounts of c-mip protein in MCNS kidney biopsy specimens and Tg(+) mice were determined as follows. Immunofluorescence staining was performed on tissue sections of the same thickness from MCNS kidney biopsy specimens and Tg(+) kidney tissues. Kidney sections from five biopsies and six three-month-old Tg(+) mice, totalling fifty glomeruli each, were analyzed. Tissue sections were viewed under a confocal laser scanning microscope LSM510-META (Carl Zeiss, Germany) with a Plan-Apochromat 63x, 1.4 numerical aperture oil immersion objective. Acquisitions were performed with an argon laser (excitation wavelength 488 nm) and fluorescence emission was collected with the META channel between 500 and 600 nm. The pinhole was set at 1.0 Airy unit (0.8 mm optical slice thickness). The images were processed with ImageJ software (http://rsb.info.nih.gov/ij/, version 1.39e). The lower and upper thresholds of fluorescence intensity (F) were fixed at 2000 and 4095 pixels, respectively. We used a high cutoff value for the lower threshold to eliminate non specific signals. The area of specific labeling (lining the capillary loops) was normalized with respect to total glomerular area (S= labeled area/total area) to account for the differences in total glomerular areas between mice and humans. This ratio was determined for each glomerulus. The semiquantification (Q) of site-specific fluorescent labeling was determined as follows: $Q = F \times S$.

Plasmid constructs, cell culture and transient transfections

A cDNA encoding c-mip was obtained from patients with MCNS and a cDNA encoding N-WASP was obtained from a podocyte cell line *(41)*. The sequences of primers and the PCR conditions are

summarized in table S4. Reverse transcription was performed with Superscript II (Invitrogen, Inc, CA) and PCR amplification was performed with the Phusion high-fidelity DNA polymerase (Finnzyme, Finland). The cDNA products were inserted into the pDonor plasmid. The full-length c-mip and N-WASP cDNAs were transferred into pDest40 by recombination (Invitrogen). The Fyn plasmids were kindly provided by Marylin D Resh (Memorial Sloan-Kettering Cancer Center) and Jacques Huot (Centre de recherche du CHUQ, Hôtel Dieu de Quebec, Canada).

Transient transfection assays were carried out in HEK 293 cells (American type Culture Collection), which were maintained in DMEM containing 10% fetal calf serum. The cells were transiently transfected by the Nanofectine-1 method, according to the instructions provided by the manufacturer (PAA, Austria). The cells were allowed to recover for 24 hours, washed three times in cold PBS, and lysed. Cells from the same number of passages were used to minimize variations in transfection efficiency.

The native recombinant c-mip was generated with the baculovirus expression system, by inserting the human *c-mip* cDNA between the BamH I and XhoI restriction sites of the transfer vector, pBacPAK9, in accordance with the manufacturer's instructions (Clontech, PaloAlto, CA). Sf9 insect cells were then cotransfected with the recombinant vector and baculovirus BacPak6 viral DNA. A high-titer recombinant viral stock was obtained and used for subsequent infection of Sf9 cells. Insect cells were infected at a multiplicity of infection of 10 in BacPAK complete medium. Ninety hours after infection, cells were harvested and lysed on ice by incubation for 5 min in complete Lysis-B, EDTA-free buffer (Roche Diagnostic GmbH, Mannheim, Germany). The recombinant c-mip was purified by a combination of preparative electrophoresis and gel electroelution (fig. 7B). The concentration of recombinant c-mip protein was determined by densitometric analysis of Coomassie Blue-stained gels containing known amounts of BSA as standard.

Immunoprecipitations and Western blot analyses

The primary antibodies used in this study included anti-phospho-Akt (Ser^{473} and Thr^{308}), anti-Akt, anti-N-WASP (Cell Signaling), anti-phospho-Fyn (Tyr^{528}, Tyr^{418}), anti-Fyn (BD Biosciences), anti-Nck

1/2, anti-Akt 1/2/3 (Santa Cruz), rabbit anti-CD2-AP (Santa Cruz Biotechnology), guinea pig anti-nephrin (Progen, Heidelberg, Germany) and rabbit anti-podocin (kindly provided by Dr. Corinne Antignac, INSERM U574, Paris, France) antibodies. The antibody against phosphorylated nephrin was provided by Dr Lawrence B. Holzman (University of Michigan Medical School, Ann Arbor, Michigan, USA). The c-mip polyclonal antibody was produced in rabbits immunized with acrylamide gel sections containing the c-mip protein. The specificity of the c-mip antibody was checked by Western blotting and IHC, by first incubating the antibody with the recombinant c-mip protein purified from supernatants of baculovorus-infected Sf9 cells. In both cases, this prior incubation resulted in an absence of signal (fig. S9, A-D). The recombinant Fyn protein was purchased from EMD Biosciences (San Diego, CA).

Cell protein extracts from podocyte or HEK 293 cells were prepared in lysis buffer B (150 mM NaCl, 10 mM Tris HCl pH 7.5, 2 mM DTT, 10% glycerol, 1 mM EDTA, 1% NP40, 1 mM protease inhibitors, 1 mM NaF, and 1 mM sodium orthovanadate).

Glomerular protein extracts were prepared in lysis buffer A (50 mM Tris HCl pH 7.5, 150 mM NaCl, 2 mM EDTA, 1% NP-40, 0.5% sodium deoxycholate, 0.1% SDS, 1 mM PMSF, 1 mM protease inhibitors, 1 mM NaF, and 1 mM sodium orthovanadate). The protein lysates were resolved by SDS-PAGE and analyzed by Western blotting with the indicated antibodies. Similar procedures were used to prepare total kidney lysates, except that the protein extracts were dialyzed overnight at 4°C in the same buffer. Immunoprecipitations were carried out with 2 mg of precleared glomerular or total kidney protein lysates and 4 μg of antibody. The complexes were precipitated with 75 μl of protein A/G sepharose (GE Healthcare Bio-science AB, Uppsala, Sweden). For coimmunoprecipitation, cell lysates containing equal amounts of protein were precleared by incuation with protein G-Sepharose for one hour at 4°C. The beads were saturated with 5% BSA for 4 hours before use. The precleared protein lysates were incubated with the appropriate antibody for 2 hours at 4°C, and 50 μl of protein G-Sepharose beads were then added and the incubation was continued overnight at 4°C. The beads were washed six times with the lysis buffer B supplemented with 0.5% NP-40 and bound proteins were resolved by SDS-PAGE, in a 10% polyacrylamide gel, transferred to nitrocellulose membranes and processed for immunoblotting. The

controls for the immunoprecipitations included the use of non immune rabbit IgG (Alpha Diagnostics Intl. Inc., San Antonio, USA) instead of primary antibody.

Generation of stable podocyte cell lines with inducible *c-mip* expression

Conditionally immortalized mouse podocytes have been described elsewhere *(41)*. Inducible podocyte cell lines were generated with the T-Rex system (Invitrogen, Life Technologies). Before transfection, podocytes were maintained at 60% confluence, under permissive conditions: RPMI 1640 medium containing 10% FCS, 100 U/ml penicillin, 100 μg/ml streptomycin, 50 U/ml γ-INF, at 33°C. Podocytes were cotransfected with a *c-mip* expression plasmid (pcDNA4/TO) and a regulatory plasmid (pcDNA6/TR) encoding the Tet repressor. In the absence of tetracycline, the Tet repressor binds to the promoter of the inducible *c-mip* expression plasmid, preventing transcription. Cotransfection was performed with 1 μg c-mip-pcDNA4/TO and 6 μg pcDNA6/TR, with the Amaxa system (Amaxa GmbH, Köhn, Germany). A plasmid encoding the LacZ gene was used as a control. After transfection, the cells were allowed to recover for 24 hours in fresh RPMI medium, under permissive conditions. Dual selection was then performed by adding blasticidin (5 μg/ml) and zeocin (125 μg/ml). Podocytes were cultured under these conditions for four weeks, for the isolation of stable cell lines expressing both the Tet repressor and *c-mip*. Differentiation was induced by maintaining stable podocyte cell lines at 37°C without γ-interferon for 14 days in the presence of blasticidin and zeocin. The expression of c-mip was induced on day 14, by adding tetracycline to the medium culture (1 μg/ml) and incubating for 48 hours. Podocytes were then lysed for protein extraction.

Generation of c-mip transgenic mice

Transgenic mice were obtained using a targeting system based on the reconstitution of a functional X-linked HPRT locus (absent from the parental embryonic stem cells), by homologous recombination, such that only embryonic stem cells with the correct integration survive HAT selection *(42)*. Three plasmids were used to construct the HPRT targeting vectors. The first, kindly provided by Chris R.J.

Kennedy (Ottawa Health Research Institute, Canada), comprises an 8.3 kb fragment of the murine promoter and the 5'-untranslated region of the nephrin gene *(43)*. The full-length coding sequence of the human *c-mip* was inserted into the XhoI site, downstream from the nephrin segment. A 13.275 kb fragment containing the transgene (nephrin segment and c-mip) was excised by digestion with NarI and PvuI. The transgene was blunted by treatment with the Klenow fragment and ligated to the EcoRI-digested, blunted and dephosphorylated-pEntr1A gateway vector, with the Quick ligase (New England Biolabs, France). The transgene was then subcloned, by homologous recombination, into the pDest vector, upstream of the promoter and the exon 1 of the human HPRT gene. The recombinant clones were checked by restriction analysis with BamHI, EcoRV and Hind II. The resulting plasmid was linearized with the AgeI restriction enzyme and micro-injected into BPES (hybrid c57BL/6 and 129) embryonic stem cells. Homologous recombinants were selected on HAT-supplemented medium containing 0.1 mM hypoxanthine, 0.0004 mM aminopterine, and 0.016 mM thymidine (Sigma Chemical, France). HAT-resistant clones were confirmed by PCR and expanded by culture for ten days. Targeted BPES (hybrid C57BL/6/129) cells were injected into wild-type blastocytes, enhancing the contribution of the embryonic stem lineage to chimera and ensuring 100% germ line transmission. Male chimeras with 100% brown coat color were crossed with wild-type (Wt) C57BL/6 females to obtain agouti offspring. Female agouti offspring were backcrossed with Wt C57BL/6 males to obtain hemizygous male mice. Successive back-crosses were performed in order to obtain a homogeneous C57BL/6 genetic background (more than five generations). Mice were genotyped by PCR analysis of tail genomic DNA. We used one pair of primers specific for the transgene (the 5' primer was located in the nephrin promoter, whereas the 3' primer was specific for c-mip) and another pair of murine primers that detects the wild-type HPRT allele in heterozygous females, but not the reconstituted HPRT allele (containing part of the human HPRT gene) in homozygous females. The sizes of the *c-mip* and *HPRT* PCR products were 817 and 300 bp, respectively.

All experiments involving animals were conducted in accordance with French laws.

Proteinuria, serum albumin and creatinine analysis

Individual mice were housed in metabolic cages (Techniplast, France). Urine was collected over a 24-hour period and this process was repeated five times for each individual. Proteinuria (mg/ml) and serum albumin and creatinine concentrations (mg/ml) were measured with the appropriate kits from Advia Chemistry 1650 (Bayer Healthcare AG, Leverkusen, Germany). The urine of neonates was analyzed with urine dipsticks (Multistix ; Bayer, Pittsburgh, Pa.). Urine samples (5 μl) were analyzed by SDS-PAGE and the gels were stained with Coomassie Brilliant Blue.

Light and electron microscopy studies

For light microscopy, kidney from wild-type and c-mip-transgenic mice were incubated for 16 hours in Dubosq-Brazil, dehydrated, embedded in paraffin, cut into sections and stained with hematoxylin and eosin (H&E) or periodic acid-Schiff (PAS) reagent. We analyzed 30 to 50 glomeruli from each mouse.

The kidney specimens used for electron microscopy were cut into small pieces, fixed by incubation with 2.5% glutaraldehyde in 0.1 M cacodylate buffer for one hour at pH 7.4, washed in the same buffer, post-fixed by incubation in 1% OsO_4 for 45 min and placed in 0.5% aqueous uranyl acetate for 1 hour at 4°C. Tissues were dehydrated in graded ethanol, infiltrated with a mixture of propylene oxide and Epon resin and embedded in Epon. Semi-thin sections were cut on an ultramicrotome (Leica, EM UC6) and stained with toluidine blue for the selection of glomeruli. Ultrathin sections were cut and post-stained with uranyl acetate and lead citrate, then examined under a Philips Tecnai 12 electron microscope. To identify targeting of endogenous c- mip in the podocyte, mice (n=3) were treated by intraperitoneal injection of LPS (200 μg in a final volume of 200 μl). Twenty-four hours later, mice were anesthetized and perfused through the left ventricule with 0.2% glutaraldehyde in 0.1 M cacodylate buffer. Kidney specimens were then processed as above.

Measurement of foot processes, glomerular basement membrane and slit pores

Negatives of electron micrographs (magnification x 6000) were scanned at a resolution of 600 dpi on an Epson Perfection 1200 Photo scanner (Epson Europe, Amsterdam). Measurements were made on the

resulting photographs with Leica QWin Pro V2.4 software (Leica Imaging Systems Ltd, Cambridge, UK). The system was calibrated using the marker bar on the electron micrographs. Five random open capillary loops in each of five randomly selected glomeruli per specimen were chosen for measurements of the length and width of the glomerular basement membrane with the image analysis software. We also manually counted the number of podocyte foot processes in each loop and expressed the results as the number of foot processes per 10 μm glomerular basement membrane length. A mean result for 25 capillary loops was obtained. For each specimen, the width of 100 individual slit pores was determined from the same set of digitized electron micrographs. Slit pore width was determined by measuring the diameter of the narrowest region of the pore between two adjacent foot processes. The width of podocyte foot processes was measured with the same marker bar on the negatives of electron micrographs. Mann-Whitney tests were used for statistical analysis.

***In vitro* activity and stability assays of Stealth RNAi (siRNA)**

We selected three sequences from the open reading frame and that are conserved between humans, rats and mice for testing in vitro. The siRNA sequences were G6 (forward strand: UCCUGCUAUGAAGAGUUCAUCAACA), G8 (forward strand: CGGACCUUUCUCAGCAAGAUCCUCA), and G10 (forward strand: AAGAGUUCAUCAACAGCCGCGACAA). The siRNA were synthesized by Invitrogen (Invitrogen, CA). The sense strand was inactivated by chemical modifications, preventing its loading into the RISc complex, thereby reducing off-target effects. To avoid a microRNA effect (siRNA binding the 3'UTR region and affecting translation), the seed region was used in a Smith-Waterman alignment analysis against human, mouse, and rat coding regions (www.invitrogen.com/rnaidesigner).

We assessed the in vitro activity of the siRNA by cotransfecting HEK cells (6 x 10^4 cells/well) with the *c-mip* expression plasmid (150 ng) and various concentrations of the siRNAs (2, 10 and 20 nM) using Lipofectamine 2000 (Invitrogen). Cells were lysed 24 hours after transfection and total RNA was purified. We quantified c-mip RNA by Q-PCR using the following forward (5'-

CTGAACGAGCTCAACGCAGGCAT-3') and reverse (5'-GACAATGTGGCTTCCTGAGACACCA-3') primers. The expression of *c-mip* was inhibited by 60% by the siRNA "G6" and by 85% for "G8" and "G10". We selected siRNA "G8" for *in vivo* experiments. The stability of siRNA and its delivery to podocytes were confirmed with an siRNA targeting cyclophilin B coupled to Alexa Fluor 647 (a gift from Dr Xavier De Mollerat, Invitrogen, CA).

siRNA treatment

Six to eight-week-old male BALB/c mice weighing 20–22 g were purchased from the Charles River Laboratory (France). Labeled (Alexa Fluor 647)-Stealth *c-mip* siRNA (10 mg/kg) was mixed with Invivofectamine (ratio: 1/1, w/v), according to the manufacturer's instructions (Invitrogen, CA) and the Invivofectamine-c-mip siRNA complex (100 μl final volume) was injected into the internal jugular vein of mice (n=10). LPS (200 μg in a final volume of 200 μl) was injected intraperitoneally into the mice 30 min after the siRNA injection. Control mice were injected with an equal amount of either LPS (n=5) or Invivofectamine alone (n=5). Mice were kept in metabolic cages and urine was collected over a 24-hour period. The mice were then killed and their kidneys were collected and processed for immunohistochemical analysis. The efficiency of siRNA delivery was determined by immunofluorescence analysis on kidney cryosections fixed in formalin. The presence and distribution of c-mip were analyzed by immunohistochemistry.

To determine whether podocyte induction of c-mip by LPS required T-cell or B-cell activation, SCID mice, which are deficient in T and B cells, were injected with LPS under similar conditions. We then analyzed the presence of c-mip by immunohistochemistry.

Statistics

The data presented are means ± SEM and were prepared with GraphPad Prism software, version 4.0. Mann-Whitney and Kruskal-Wallis tests were used to evaluate the significance of differences. Values of $P < 0.05$ were considered significant.

Supplementary Materials

Table S1. Characteristics of the patients at the time of biopsy.

Table S2. Quantification of c-mip abundance in glomeruli of kidney tissues from MCNS patients and Tg(+) mice.

Table S3. Semi-quantitative measurement of urinary protein concentration in newborn transgenic mice.

Table S4. Sequence of primers and PCR conditions.

Figure S1. Representative *in situ* hybridization of serial sections from kidney biopsy specimens from patients with MN and FSGS.

Figure S2. Detection of c-mip in other glomerular diseases.

Figure S3. Generation of c-mip transgenic mice**.**

Figure S4. Histological, functional and immuno-ultrastructural studies of c-mip transgenic mice.

Figure S5. Morphological characterization of c-mip transgenic mice.

Figure S6. Quantification of confocal microscopy results for c-mip abundance in glomeruli from kidney tissue from MCNS patients and Tg(+) mice.

Figure S7. Ultrastructural analysis of podocytes from five-day-old newborn transgenic mice.

Figure S8. Course of glomerular disease in c-mip Tg mice.

Figure S9. Confocal microscopy analysis of the abundance of phosphorylated nephrin (red) and total nephrin (green) in kidney sections from eight-week-old wt and Tg(+) mice.

Figure S10. Quantification of confocal microscopy results concerning the phosphorylation of Ser^{473} in Akt in glomerular diseases.

Figure S11. Specificity of the anti-c-mip antibody.

Figure S12. Interactions of c-mip with Fyn and N-WASP

Figure S13. Immunogold labeling of c-mip in LPS-treated mice

References and Notes

1. L. A. Stevens, A. S. Levey, Measured GFR as a confirmatory test for estimated GFR. *J Am Soc Nephro*l. 20, 2305-2313 (2009).
2. K. Tryggvason, J. Patrakka, J. Wartiovaara, Hereditary proteinuria syndromes and mechanisms of proteinuria. *N Engl J Med*. 354, 1387-1401 (2006).
3. D. Kerjaschki, Caught flat-footed: podocyte damage and the molecular bases of focal glomerulosclerosis. *J Clin Invest*. 108, 1583-1587 (2001).
4. T. Benzing, Signaling at the slit diaphragm. *J Am Soc Nephrol* 15, 1382-1391 (2004).
5. M. Kestila, U. Lenkkeri, M. Mannikko, J. Lamerdin, P. McCready, H. Putaala, V. Ruotsalainen, T. Morita, M. Nissinen, R. Herva, C. E. Kashtan, L. Peltonen, C. Holmberg, A. Olsen, K. Tryggvason, Positionally cloned gene for a novel glomerular protein--nephrin--is mutated in congenital nephrotic syndrome. *Mol Cell.* 1, 575-582. (1998).
6. N. Boute, O. Gribouval, S. Roselli, F. Benessy, H. Lee, A. Fuchshuber, K. Dahan, M. C. Gubler, P. Niaudet, C. Antignac, NPHS2, encoding the glomerular protein podocin, is mutated in autosomal recessive steroid-resistant nephrotic syndrome. *Nat Genet.* 24, 349-354. (2000).
7. J. M. Kim, H. Wu, G. Green, C. A. Winkler, J. B. Kopp, J. H. Miner, E. R. Unanue, A. S. Shaw, CD2-associated protein haploinsufficiency is linked to glomerular disease susceptibility. *Science.* 300, 1298-1300 (2003).
8. J. M. Kaplan, S. H. Kim, K. N. North, H. Rennke, L. A. Correia, H. Q. Tong, B. J. Mathis, J. C. Rodriguez-Perez, P. G. Allen, A. H. Beggs, M. R. Pollak, Mutations in ACTN4, encoding alpha-actinin-4, cause familial focal segmental glomerulosclerosis. *Nat Genet*. 24, 251-256. (2000).
9. J. Reiser, K. R. Polu, C. C. Moller, P. Kenlan, M. M. Altintas, C. Wei, C. Faul, S. Herbert, I. Villegas, C. Avila-Casado, M. McGee, H. Sugimoto, D. Brown, R. Kalluri, P. Mundel, P. L.

Smith, D. E. Clapham, M. R. Pollak, TRPC6 is a glomerular slit diaphragm-associated channel required for normal renal function. *Nat Genet*. 37, 739-744 (2005).

10. B. Hinkes, R. C. Wiggins, R. Gbadegesin, C. N. Vlangos, D. Seelow, G. Nurnberg, P. Garg, R. Verma, H. Chaib, B. E. Hoskins, S. Ashraf, C. Becker, H. C. Hennies, M. Goyal, B. L. Wharram, A. D. Schachter, S. Mudumana, I. Drummond, D. Kerjaschki, R. Waldherr, A. Dietrich, F. Ozaltin, A. Bakkaloglu, R. Cleper, L. Basel-Vanagaite, M. Pohl, M. Griebel, A. N. Tsygin, A. Soylu, D. Muller, C. S. Sorli, T. D. Bunney, M. Katan, J. Liu, M. Attanasio, F. O'Toole J, K. Hasselbacher, B. Mucha, E. A. Otto, R. Airik, A. Kispert, G. G. Kelley, A. V. Smrcka, T. Gudermann, L. B. Holzman, P. Nurnberg, F. Hildebrandt, Positional cloning uncovers mutations in PLCE1 responsible for a nephrotic syndrome variant that may be reversible. *Nat Genet*. 38, 1397-1405 (2006).

11. J. Patrakka, K. Tryggvason, Nephrin- a unique structural and signaling protein of the kidney filter. *Trends Mol Med*. 13, 396-403 (2007).

12. R. Verma, I. Kovari, A. Soofi, D. Nihalani, K. Patrie, L. B. Holzman, Nephrin ectodomain engagement results in Src kinase activation, nephrin phosphorylation, Nck recruitment, and actin polymerization. *J Clin Invest*. 116, 1346-1359 (2006).

13. N. Jones, I. M. Blasutig, V. Eremina, J. M. Ruston, F. Bladt, H. Li, H. Huang, L. Larose, S. S. Li, T. Takano, S. E. Quaggin, T. Pawson, Nck adaptor proteins link nephrin to the actin cytoskeleton of kidney podocytes. *Nature*. 440, 818-823 (2006).

14. T. B. Huber, B. Hartleben, J. Kim, M. Schmidts, B. Schermer, A. Keil, L. Egger, R. L. Lecha, C. Borner, H. Pavenstadt, A. S. Shaw, G. Walz, T. Benzing, Nephrin and CD2AP associate with phosphoinositide 3-OH kinase and stimulate AKT-dependent signaling. *Mol Cell Biol*. 23, 4917-4928 (2003).

15. H. N. Higgs, T. D. Pollard, Regulation of actin filament network formation through ARP2/3 complex: activation by a diverse array of proteins. *Annu Rev Biochem*. 70, 649-676 (2001).

16. S. Banin, O. Truong, D. R. Katz, M. D. Waterfield, P. M. Brickell, I. Gout, Wiskott-Aldrich syndrome protein (WASp) is a binding partner for c-Src family protein-tyrosine kinases. *Curr Biol.* 6, 981-988 (1996).

17. T. B. Huber, C. Kwoh, H. Wu, K. Asanuma, M. Godel, B. Hartleben, K. J. Blumer, J. H. Miner, P. Mundel, A. S. Shaw, Bigenic mouse models of focal segmental glomerulosclerosis involving pairwise interaction of CD2AP, Fyn, and synaptopodin. *J Clin Invest*. 116, 1337-1345 (2006).

18. D. Sahali, A. Pawlak, A. Valanciute, P. Grimbert, P. Lang, P. Remy, A. Bensman, G. Guellen, A novel approach to investigation of the pathogenesis of active minimal- change nephrotic syndrome using subtracted cDNA library screening. *J Am Soc Nephrol*. 13, 1238-1247. (2002).

19. A. A. Eddy, J. M. Symons, Nephrotic syndrome in childhood. *Lancet*. 362, 629-639 (2003).

20. C. Kitiyakara, J. B. Kopp, P. Eggers, *Trends in the epidemiology of focal segmental glomerulosclerosis*. *Semin Nephrol*. 23, 172-182 (2003).

21. A. Meyrier, Nephrotic focal segmental glomerulosclerosis in 2004: an update. *Nephrol Dial Transplant*. 19, 2437-2444 (2004).

22. V. D. D'Agati, A. B. Fogo, J. A. Bruijn, J. C. Jennette, Pathologic classification of focal segmental glomerulosclerosis: a working proposal. *Am J Kidney Dis*. 43, 368-382 (2004).

23. P. W. Mathieson, Minimal change nephropathy and focal segmental glomerulosclerosis. *Semin Immunopathol.* 29, 415-426 (2007).

24. P. Ronco, H. Debiec, Molecular pathomechanisms of membranous nephropathy: from Heymann nephritis to alloimmunization. *J Am Soc Nephrol*. 16, 1205-1213 (2005).

25. J. P. DiNitto, D. G. Lambright, Membrane and juxtamembrane targeting by PH and PTB domains. *Biochim Biophys Acta.* 1761, 850-867 (2006).

26. D. Filipp, J. Zhang, B. L. Leung, A. Shaw, S. D. Levin, A. Veillette, M. Julius, Regulation of Fyn through translocation of activated Lck into lipid rafts. *J Exp Med.* 197, 1221-1227 (2003).

27. H. N. Higgs, T. D. Pollard, Activation by Cdc42 and PIP(2) of Wiskott-Aldrich syndrome protein (WASp) stimulates actin nucleation by Arp2/3 complex. *J Cell Biol.* 150, 1311-1320 (2000).

28. D. Kerjaschki, T. J. Neale, Molecular mechanisms of glomerular injury in rat experimental membranous nephropathy (Heymann nephritis). *J Am Soc Nephrol*. 7, 2518-2526 (1996).

29. L. H. Noel, M. Zanetti, D. Droz, C. Barbanel, Long-term prognosis of idiopathic membranous glomerulonephritis. Study of 116 untreated patients. *Am J Med*. 66, 82-90 (1979).

30. P. L. Leenaerts, B. M. Hall, B. J. Van Damme, M. R. Daha, Y. F. Vanrenterghem, Active Heymann nephritis in complement component C6 deficient rats. *Kidney Int*. 47, 1604-1614 (1995).

31. S. T. Spicer, G. T. Tran, M. C. Killingsworth, N. Carter, D. A. Power, K. Paizis, R. Boyd, S. J. Hodgkinson, B. M. Hall, Induction of passive Heymann nephritis in complement component 6-deficient PVG rats. *J Immunol.* 179, 172-178 (2007).

32. S. P. Makker, J. J. Kanalas, Course of transplanted Heymann nephritis kidney in normal host. Implications for mechanism of proteinuria in membranous glomerulonephropathy. *J Immunol.* 142, 3406-3410 (1989).

33. S. Doublier, V. Ruotsalainen, G. Salvidio, E. Lupia, L. Biancone, P. G. Conaldi, P. Reponen, K. Tryggvason, G. Camussi, Nephrin redistribution on podocytes is a potential mechanism for proteinuria in patients with primary acquired nephrotic syndrome. *Am J Pathol*. 158, 1723-1731 (2001).

34. L. J. Shih NY, Karpitskii V, Nguyen A, Dustin ML, Kanagawa O, Miner JH, Shaw AS., Congenital nephrotic syndrome in mice lacking CD2-associated protein. *Science.* 286, 312-315 (1999).

35. C. C. Yu, T. S. Yen, C. A. Lowell, A. L. DeFranco, Lupus-like kidney disease in mice deficient in the Src family tyrosine kinases Lyn and Fyn. *Curr Biol*. 11, 34-38 (2001).

36. I. Quack, L. C. Rump, P. Gerke, I. Walther, T. Vinke, O. Vonend, T. Grunwald, L. Sellin, beta-Arrestin2 mediates nephrin endocytosis and impairs slit diaphragm integrity. *Proc Natl Acad Sci U S A.* 103, 14110-14115 (2006).

37. N. Jones, L. A. New, M. A. Fortino, V. Eremina, J. Ruston, I. M. Blasutig, L. Aoudjit, Y. Zou, X. Liu, G. L. Yu, T. Takano, S. E. Quaggin, T. Pawson, Nck proteins maintain the adult glomerular filtration barrier. *J Am Soc Nephrol.* 20, 1533-1543 (2009).

38. J. Reiser, G. von Gersdorff, M. Loos, J. Oh, K. Asanuma, L. Giardino, M. P. Rastaldi, N. Calvaresi, H. Watanabe, K. Schwarz, C. Faul, M. Kretzler, A. Davidson, H. Sugimoto, R. Kalluri, A. H. Sharpe, J. A. Kreidberg, P. Mundel, Induction of B7-1 in podocytes is associated with nephrotic syndrome. *J Clin Invest.* 113, 1390-1397 (2004).

39. Y. Sun, L. He, M. Takemoto, J. Patrakka, T. Pikkarainen, G. Genove, J. Norlin, K. Truve, K. Tryggvason, C. Betsholtz, Glomerular Transcriptome Changes Associated with Lipopolysaccharide-Induced Proteinuria. *Am J Nephrol.* 29, 558-570 (2009).

40. S. Y. Zhang, A. Marlier, O. Gribouval, T. Gilbert, L. Heidet, C. Antignac, M. C. Gubler, In vivo expression of podocyte slit diaphragm-associated proteins in nephrotic patients with NPHS2 mutation. *Kidney Int.* 66, 945-954 (2004).

41. P. Mundel, J. Reiser, A. Zuniga Mejia Borja, H. Pavenstadt, G. R. Davidson, W. Kriz, R. Zeller, Rearrangements of the cytoskeleton and cell contacts induce process formation during differentiation of conditionally immortalized mouse podocyte cell lines. *Exp Cell Res.* 236, 248-258 (1997).

42. S. K. Bronson, E. G. Plaehn, K. D. Kluckman, J. R. Hagaman, N. Maeda, O. Smithies, Single-copy transgenic mice with chosen-site integration. *Proc Natl Acad Sci U S A.* 93, 9067-9072 (1996).

43. J. L. Michaud, L. I. Lemieux, M. Dube, B. C. Vanderhyden, S. J. Robertson, C. R. Kennedy, Focal and segmental glomerulosclerosis in mice with podocyte-specific expression of mutant alpha-actinin-4. *J Am Soc Nephrol.* 14, 1200-1211 (2003).

Acknowledgments

We would like to thank Dr Chris R.J. Kennedy (Ottawa Health Research Institute, Ontario, Canada) for providing the nephrin promoter, Dr Marylin D Resh (Department of Cell Biology and Genetics, Memorial Sloan-Kettering Cancer Center, New York, USA) and Dr Jacques Huot (Centre de recherche de L'Hôtel-Dieu de Québec, Canada) for providing the Fyn plasmids, Dr Peter Mundel (Mount Sinai School of Medicine, New York, USA) for providing the podocyte cell line, Dr Thomas Benzing (Renal Division, University Hospital Freiburg, Freiburg, Germany) for providing the nephrin plasmid, Dr Corinne Antignac (INSERM U574, Hôpital Necker Enfant-Malades, Paris, France) for providing the anti-podocin antibody and Dr Lawrence Holzman (Medical Science Research, Ann Arbor, USA) for providing the anti-phosphorylated nephrin antibody. We thank Dr Xavier de Mollerat (Invitrogen, CA) for technical assistance with RNAi experiments and for providing us with the cyclophilin-targeting siRNA. We thank Dr Esmilaire Liliane (Biochemistry Department, Henri Mondor Hospital) for biochemical determinations, Laurence Kheuang, Virginie Fataccioli and Aurore Manceau (Pathology Department) for technical assistance with electron microscopy. We thank Yves Allory (Pathology Department) for providing us with renal samples. We thank Rachid Souktani (the animal facility laboratory at the IRMB, Créteil) for assistance with microinjection experiments in mice.

This work was supported in part by an Avenir Program from INSERM, a grant from the French Kidney Foundation, Association pour l'Utilisation du Rein Artificiel (AURA) and Assistance Publique des Hôpitaux de Paris, AP-HP (Programme hospitalier de recherche clinique).

Legends

Fig. 1. The abundance of c-mip increases in the glomeruli of patients with MCNS. **(A)** Representative immunohistochemical analysis of serial sections from normal human kidney (NHK) and kidney biopsy specimens from patients with MCNS relapse. Scale bars, 20 μM **(B)** Confocal microscopy analysis of nephrin (red) and c-mip (green) expression in normal human kidney tissues (upper panel) and MCNS biopsies (lower panel). The basal amount of c-mip was below the limit of detection, whereas c-mip was visualized along the peripheral capillary loops in patients with MCNS. The c-mip and nephrin were colocalized in the glomerulus. Scale bars, 10 μM.

Fig. 2. Stable overexpression of *c-mip* in podocytes induces phenotypic alterations. **(A)** Confocal microscopy analysis of phalloidin staining. *c-mip*–overexpressing podocytes display a loss of stress fibers, whereas the actin network is well preserved in non-induced stable *c-mip* transfectants. Scale bars, 10 μM. **(B)** Western blot of protein lysates from non-induced (-) and induced (+) *c-mip* stable transfectants. The induction of c-mip inhibits the phosphorylation of nephrin and triggers the inactivation of Fyn and Akt. Data from two independent experiments are shown.

Fig. 3. c-mip transgenic mice develop nephrotic proteinuria without inflammatory lesions or cell infiltrations. **(A)** Proteinuria was assessed by the proteinuria/creatinine ratio (Upr/Ucr). Upr/Ucr was 3.5 ± 0.75 in eight-week-old female heterozygotes (Tg+/-, n=26 mice), 61 ± 12.5 in male hemizygote Tg(+) transgenic mice (n=34 mice) and 2.6 ± 0.5 wild-type (WT) mice (n=12 mice). **(B)** Urine samples (5 μl) and BSA (15 μg) were resolved by SDS-PAGE and gels stained with Coomassie Blue. **(C)** Kidney sections from eight-week-old c-mip transgenic mice were examined. Tg(+) mice display podocyte flattening and the effacement of foot processes. The effacement of foot processes is associated with the disappearance of slit diaphragms, which are replaced by occluding junctions (arrow). Scale bars, Tg(+):

upper and middle micrographs, 0.5 μM; lower micrograph, 0.1 μM. **(D);** The foot processes are evenly spaced in wild-type mice. Scale bars, upper micrograph, 1 μM; lower microgaph, 0.1 μM. **(E)** Morphometric analysis of foot process effacement indicating that the width of the podocyte sole in Tg(+) mice is twice that in the wild-type. N=3 mice per genotype were analyzed. Data are means ± SEM. Mann-Whitney test, * P <0.05.

Fig. 4. Podocytes of c-mip transgenic mice have an abnormal phenotype. **(A)** Immunoprecipitation of nephrin from two different Tg(+) glomerular lysates, followed by Western blotting for phosphorylated nephrin and total nephrin. The amount of phosphorylated nephrin is reduced (right panel). Data from two independent experiments are shown. **(B)** Western-blot analysis of glomerular protein lysates from 10-week-old wild-type mice and Tg(+) mice**.** Fyn is mostly present in the inactive form, whereas the amount of $pSer^{473}$-Akt is reduced. Data from two independent experiments are shown. **(C)** Lower abundance of phosphorylated Akt ($pSer^{473}$-Akt) in the glomeruli (G) of patients with MCNS disease and in Tg(+) mice than in normal human kidney (NHK) and wild-type mice, respectively. Scale bars, 10 μM.

Fig. 5. Interactions between nephrin, Nck and N-WASP are altered in c-mip Tg(+) mice. Immunoprecipitation (IP) of Fyn, N-WASP, and Nck from glomerular lysates of wild-type and Tg(+) mice. **(A)** c-mip coimmunoprecipitates with Fyn in Tg(+) glomerular lysates. **(B)** The amount of nephrin present in Fyn complexes is lower in glomerular lysates from Tg(+) mice than in those from wild-type mice. **(C)** The interactions of N-WASP with Fyn is decreased in Tg(+) mice compared to wild-type mice. **(D)** Immunoprecipitation of Nck from wild-type and Tg(+) glomerular lysates, followed by Western blotting with an anti-nephrin antibody. The interactions of Nck with nephrin are decreased in Tg(+) mice compared to wild-type mice. **(E)** Immunoprecipitation of nephrin from three different Tg(+) glomerular lysates, followed by Western blotting with anti-Nck antibody. The interaction of nephrin with Nck is reduced in Tg(+) mice compared to wild-type mice. Reprobing with an antibody against nephrin showed that equal amounts of nephrin were immunoprecipitated.

Fig. 6. Knockdown of c-mip prevents the development of nephrotic proteinuria. **(A)** Detection of c-mip in LPS-treated Balb/c mice. Immunohistochemistry analysis showing a greater abundance of c-mip in podocytes (upper panel). Scale bars, 20 μM. Immunoprecipitation of glomerular extracts from LPS-treated mice with anti-Fyn or mouse IgG (lower panel). **(B)** Increased abundance of c-mip in the podocytes of LPS-treated SCID mice than in those of untreated SCID mice. Scale bars, 20 μM. **(C)** Effects of c-mip siRNA injection in LPS-treated Balb/c mice. Balb/c mice (n=10 mice) received a single injection of c-mip siRNA (10 mg/kg) coupled to Alexa Fluor 647 into the internal jugular vein, and after 30 min, were injected intraperitoneally with LPS (200 μg). Controls include mice injected with LPS (n=5 mice) or Invivofectamine (n=5 mice) and non-injected mice (NI, n=5 mice). Urine was collected over a 24-hour period and the kidneys were harvested and processed for immunohistochemistry. Alexa Fluor 647 staining of kidney sections demonstrated that c-mip-siRNA duplexes were delivered to podocytes (upper panel). Scale bars, 10 μM. Immunohistochemistry analysis showed that mice treated with LPS and c-mip siRNA contained less c-mip than mice treated with LPS only (middle panel). Scale bars, 10 μM. RT-qPCR analysis of *c-mip* expression in mouse kidney (lower panel, left). mRNA abundance is expressed with respect to glyceraldehyde-3-phosphate deshydrogenase (GAPDH). Data are means ± SEM ($p<0.05$, Kruskal-Wallis test). Proteinuria was significantly lower in c-mip siRNA-treated mice than in mice treated with LPS alone ($p=0.0017$, Kruskal-Wallis test) (lower panel, left).

Figure 7. c-mip siRNA prevents the inactivation of nephrin and Akt. (A) Confocal microscopy analysis of phosphorylated nephrin (green) and total nephrin (red) in kidney sections. The relative abundances of nephrin and phosphorylated nephrin were assessed by quantifying the specific glomerular fluorescence intensity (lining the capillary loops) in three-dimensional stacks of images taken by confocal microscopy and normalized with respect to total glomerular area. Twenty glomeruli were analyzed for each set of conditions. The data presented are means ± SEM. The amount of phosphorylated nephrin was lower in LPS-treated mice than in siRNA-treated mice. The decrease in nephrin abundance is less marked in these mice. Scale bars, 10 μM. **(B)** Confocal microscopy analysis of phosphorylated Akt ($pSer^{473}$-Akt) in kidney sections from mice treated with LPS alone or with LPS and siRNA. Scale bars, 10 μM. Data are

means ± SEM. The amount of $pSer^{473}$-Akt is significantly lower in LPS-treated mice (n=3 mice), than in LPS- and siRNA-treated mice (n=3 mice) (20 glomeruli were analyzed per mouse, $p < 0.05$, Kruskal-Wallis test).

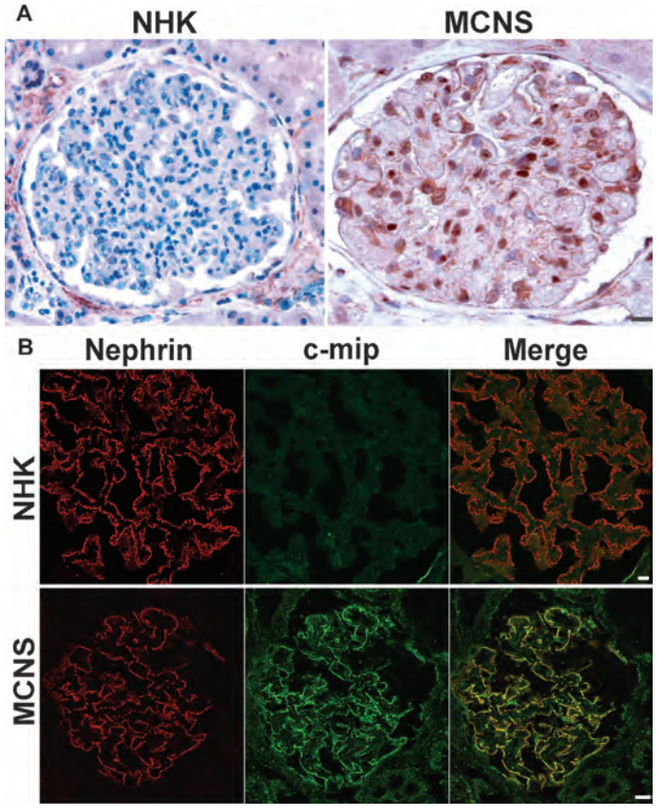
A
NHK
MCNS
B
Nephrin
c-mip
Merge
NHK
MCNS

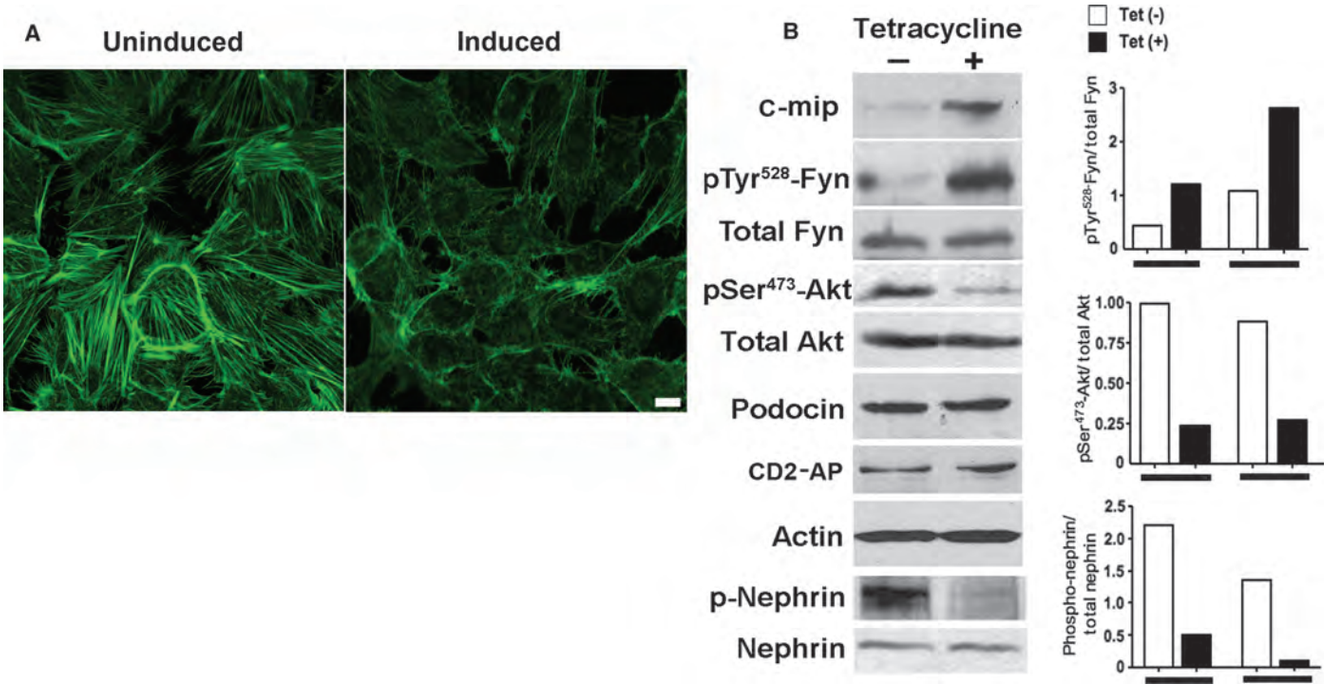
A
Uninduced
Induced
B
Tetracycline
–
+
c-mip
pTyr528-Fyn
Total Fyn
pSer473-Akt
Total Akt
Podocin
CD2-AP
Actin
p-Nephrin
Nephrin
Tet (-)
Tet (+)
pTyr528-Fyn/ total Fyn
pSer473-Akt/ total Akt
Phospho-nephrin/ total nephrin

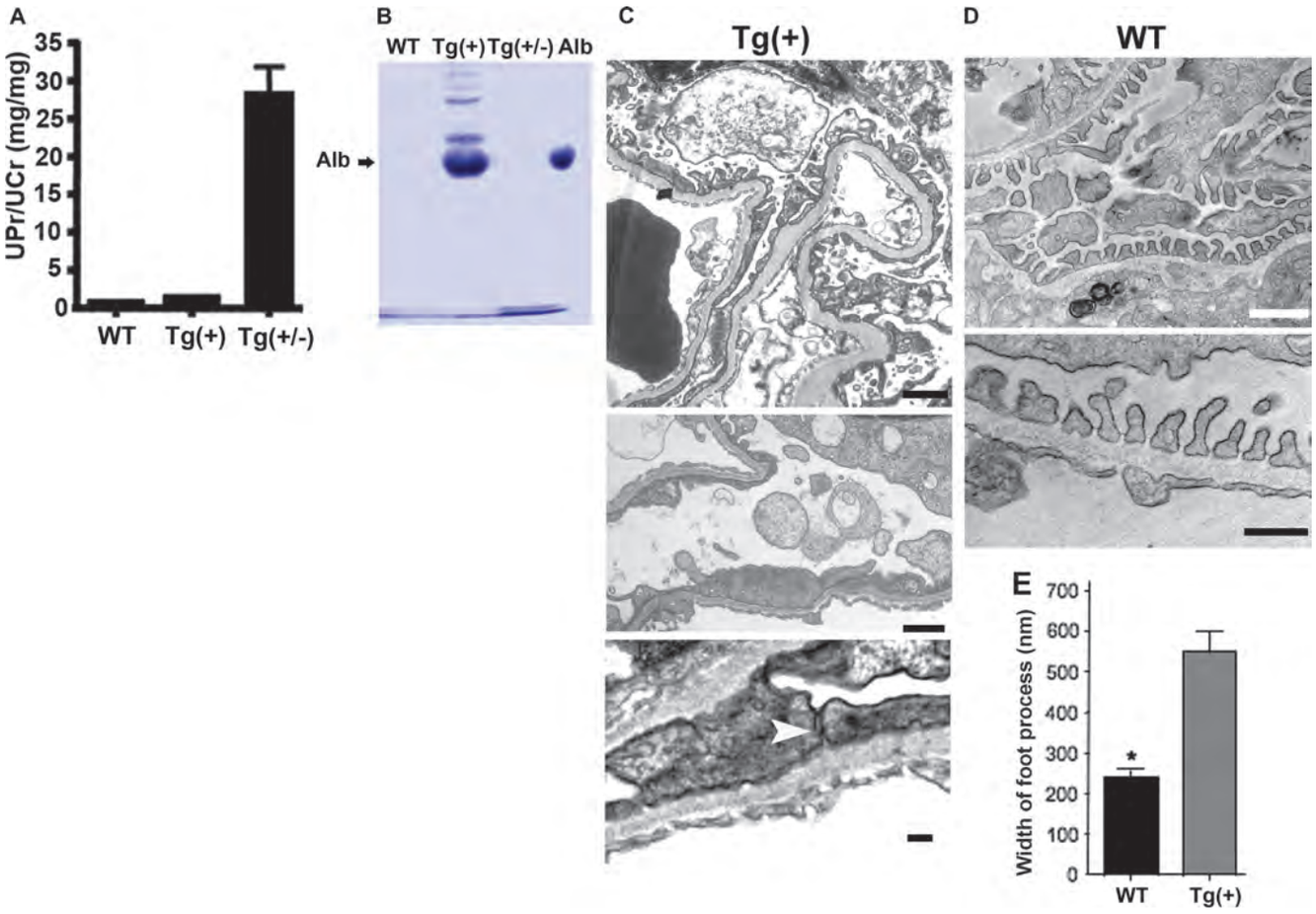
A
UPr/UCr (mg/mg)
35
30
25
20
15
10
5
0
WT
Tg(+)
Tg(+/-)
B
WT Tg(+) Tg(+/-) Alb
Alb
C
Tg(+)
D
WT
E
Width of foot process (nm)
700
600
500
400
300
200
100
0
*
WT
Tg(+)

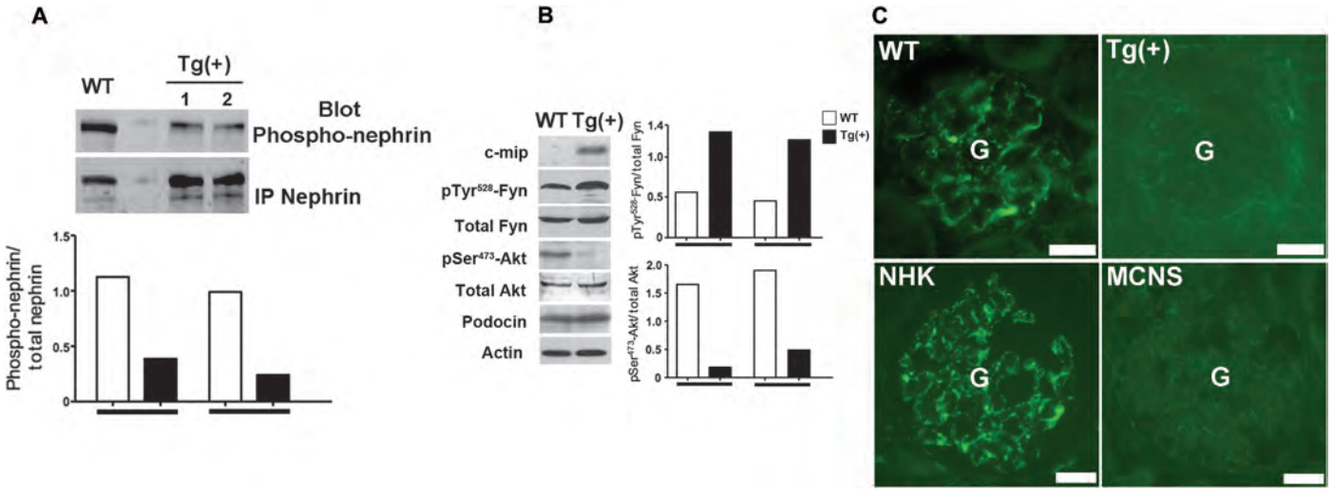
A
WT
Tg(+)
1
2
Blot
Phospho-nephrin
IP Nephrin
Phospho-nephrin/
total nephrin
1.5
1.0
0.5
0
B
WT Tg(+)
c-mip
pTyr528-Fyn
Total Fyn
pSer473-Akt
Total Akt
Podocin
Actin
pTyr528-Fyn/total Fyn
1.4
1.0
0.5
0
WT
Tg(+)
pSer473-Akt/total Akt
2.0
1.5
1.0
0.5
0
C
WT
Tg(+)
NHK
MCNS
G

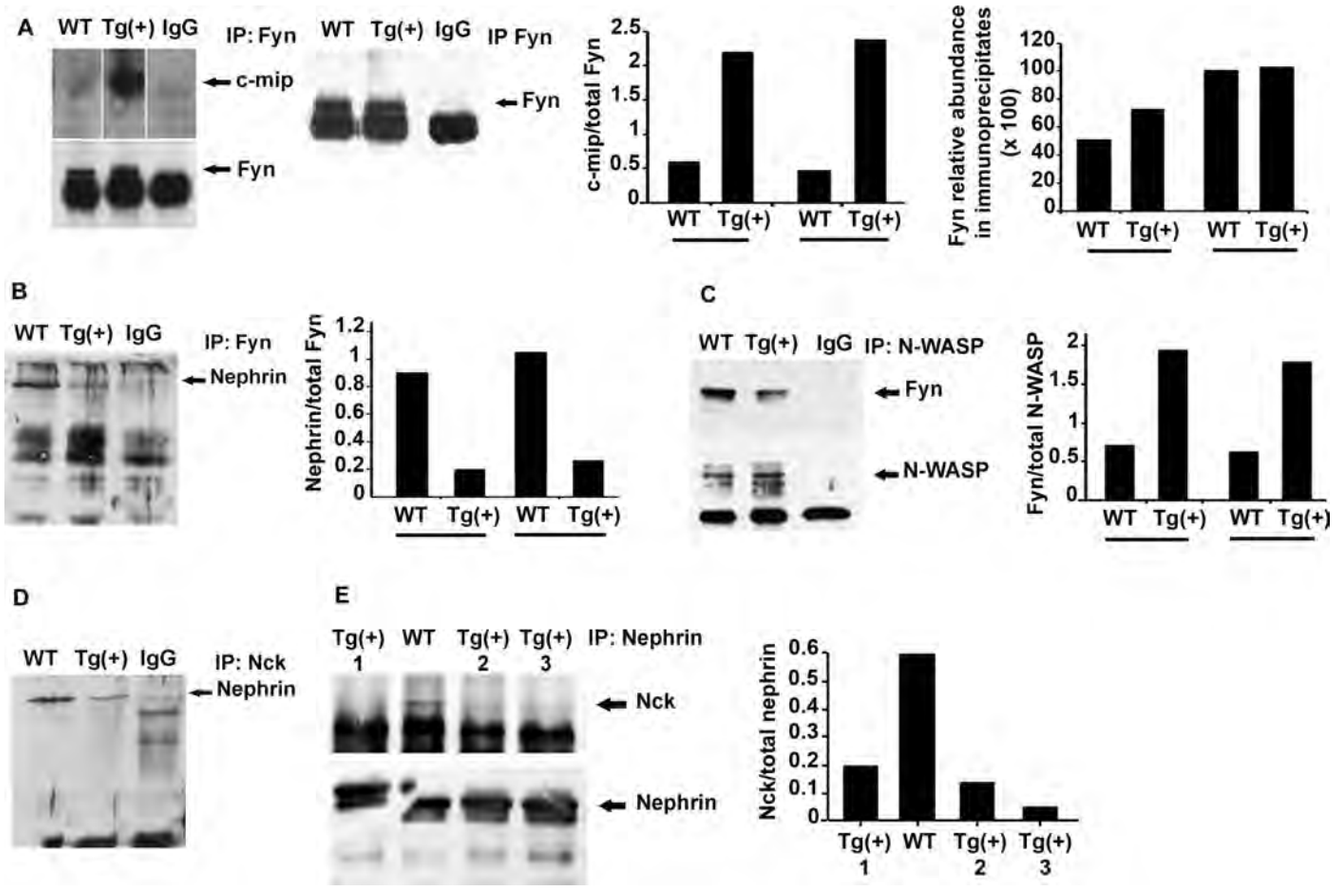
A
WT Tg(+) IgG
IP: Fyn
c-mip
Fyn
WT Tg(+) IgG
IP Fyn
Fyn
c-mip/total Fyn
2.5
2
1.5
1
0.5
0
WT Tg(+) WT Tg(+)
Fyn relative abundance in immunoprecipitates (x 100)
120
100
80
60
40
20
0
WT Tg(+) WT Tg(+)
B
WT Tg(+) IgG
IP: Fyn
Nephrin
Nephrin/total Fyn
1.2
1
0.8
0.6
0.4
0.2
0
WT Tg(+) WT Tg(+)
C
WT Tg(+) IgG
IP: N-WASP
Fyn
N-WASP
Fyn/total N-WASP
2
1.5
1
0.5
0
WT Tg(+) WT Tg(+)
D
WT Tg(+) IgG
IP: Nck
Nephrin
E
Tg(+) 1
WT
Tg(+) 2
Tg(+) 3
IP: Nephrin
Nck
Nephrin
Nck/total nephrin
0.6
0.5
0.4
0.3
0.2
0.1
0
Tg(+) 1
WT
Tg(+) 2
Tg(+) 3

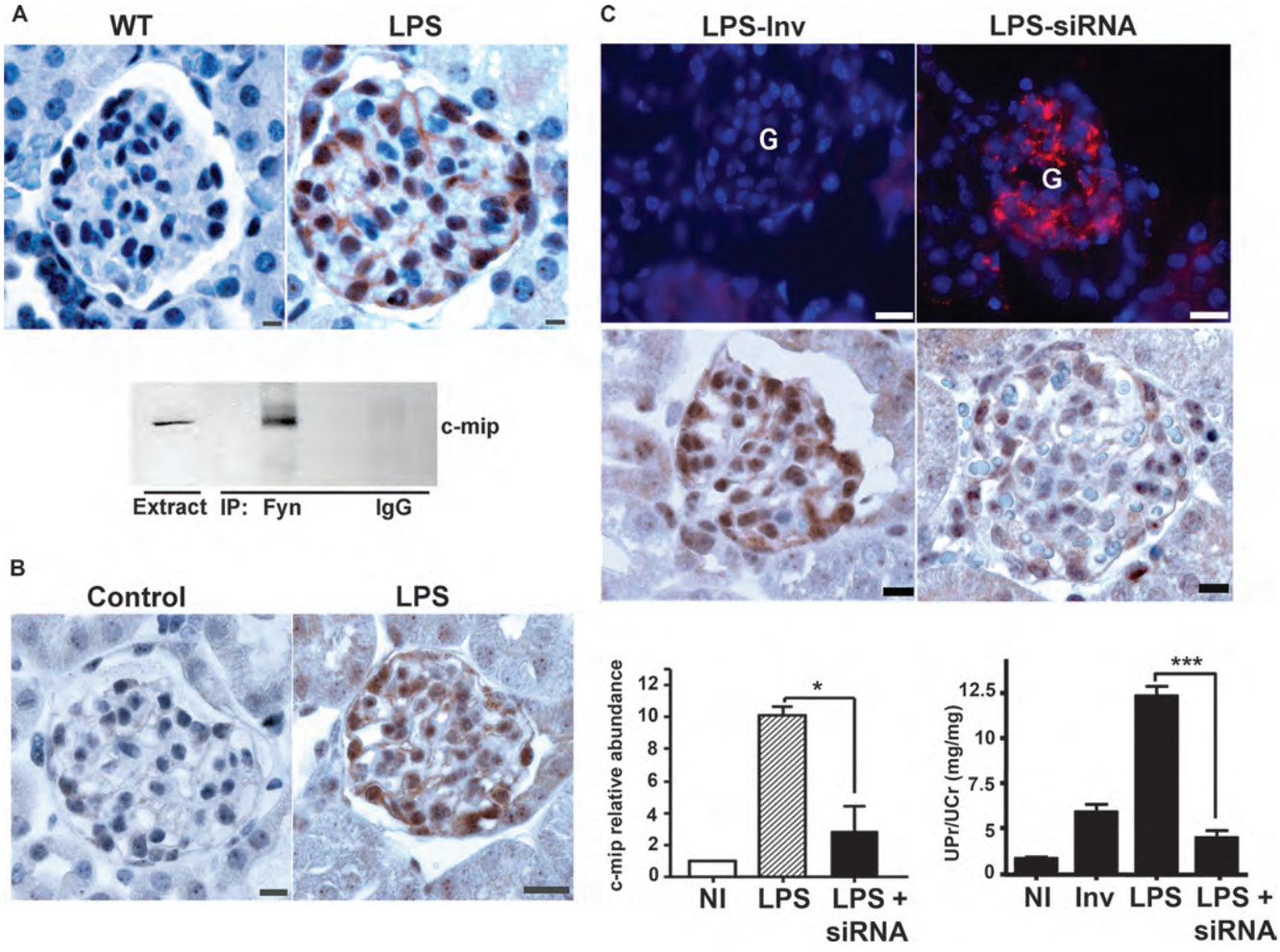
A
WT
LPS
c-mip
Extract
IP: Fyn
IgG
B
Control
LPS
C
LPS-Inv
LPS-siRNA
G
G
c-mip relative abundance
12
10
8
6
4
2
0
*
NI
LPS
LPS + siRNA
UPr/UCr (mg/mg)
12.5
10
7.5
5
0
***
NI
Inv
LPS
LPS + siRNA

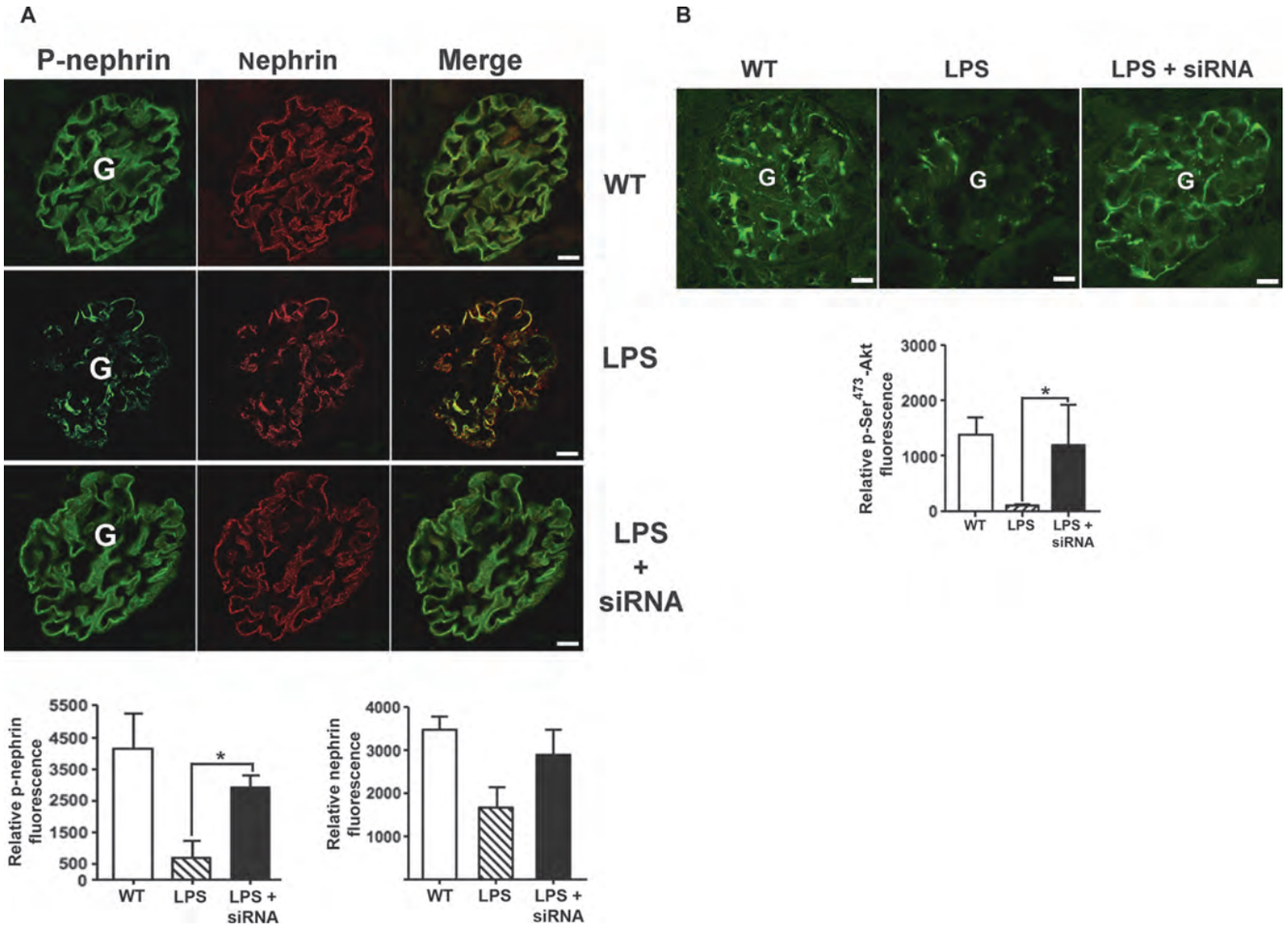
A
P-nephrin
Nephrin
Merge
G
WT
LPS
LPS + siRNA
Relative p-nephrin fluorescence
5500
4500
3500
2500
1500
500
0
*
WT
LPS
LPS + siRNA
Relative nephrin fluorescence
4000
3000
2000
1000
B
WT
LPS
LPS + siRNA
Relative p-Ser473-Akt fluorescence
3000
2000
1000
0

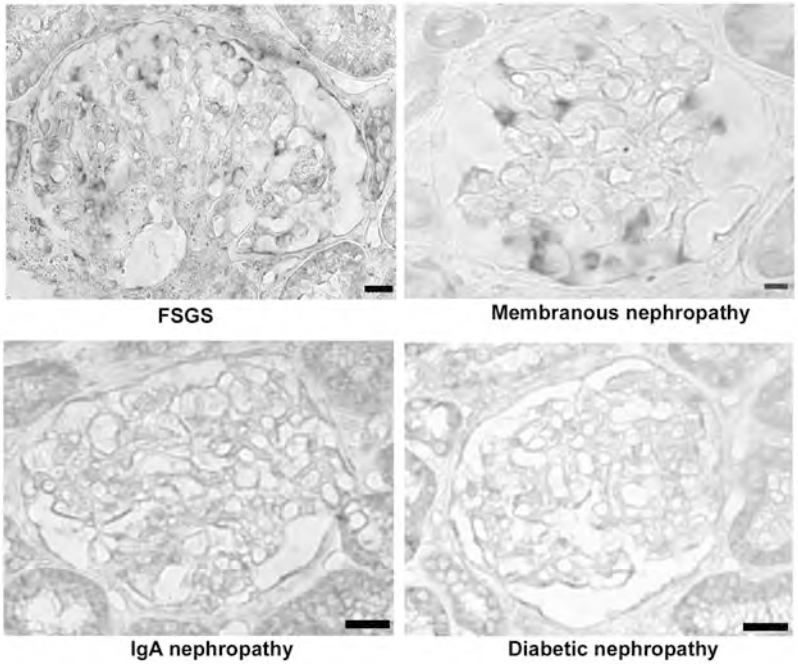

Figure S1. Representative in situ hybridization of serial sections from kidney biopsies from patients with MN and FSGS. c-mip was detected in biopsies from patients with FSGS and MN but not in those with IgA nephropathy and in diabetic nephropathy.

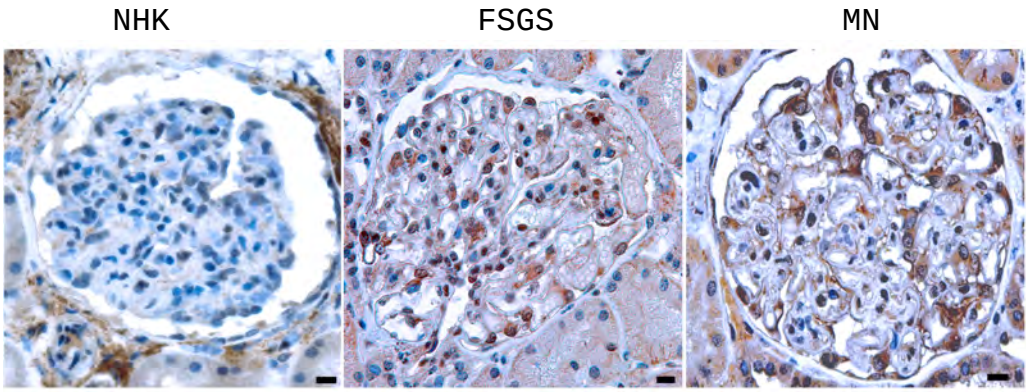

Figure S2. Detection of c-mip in other glomerular diseases. The abundance of c-mip is increased in glomeruli of patients with FSGS and MN.Scale bars,20 μM

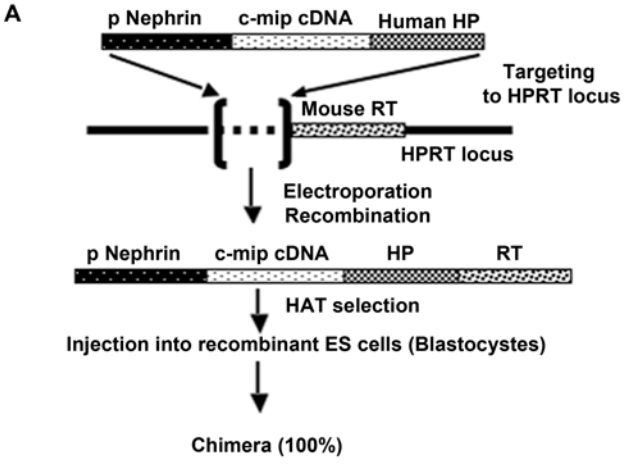
A
p Nephrin
c-mip cDNA
Human HP
Targeting
to HPRT locus
Mouse RT
HPRT locus
Electroporation
Recombination
p Nephrin
c-mip cDNA
HP
RT
HAT selection
Injection into recombinant ES cells (Blastocystes)
Chimera (100%)

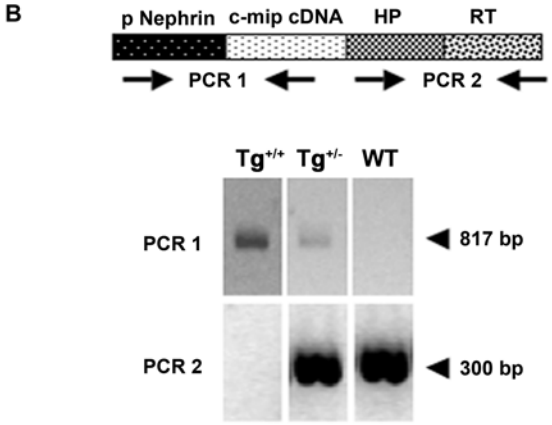
B
p Nephrin
c-mip cDNA
HP
RT
PCR 1
PCR 2
Tg+/+
Tg+/-
WT
PCR 1
817 bp
PCR 2
300 bp

Figure S3. Generation of c-mip transgenic mice. (**A)** Schematic diagram of constructs used for podocyte-specific expression of the human c-mip transgene. The full-length coding sequence of human c-mip was inserted downstream of the murine nephrin promoter (pNephrin). The plasmid construct (containing the pNephrin-c-mip construct) was then subcloned by homologous recombination into the pDest vector, upstream of the human Hprt sequence (HP) containing the promoter and the exon 1. The resulting plasmid containing the transgene (pNephrin-c-mip-human HP) was linearized and microinjected into BPES (hybrid C57BL/6 and 129) ES cells. The homologous recombination between the BPES HPRT locus and the targeting vector results in the integration of a single copy of a human c-mip at the HPRT locus. Homologous recombinants were selected on HAT-supplemented medium. HAT-resistant clones were confirmed by PCR and then injected into wild-type blastocyts. We obtained eleven 100% chimeric male founders from three independent BPES clones. The transgene was expressed in males and females following Mendelian sex-linked segregation. A 300-bp PCR product specific to the endogenous Hprt gene was detected only in heterozygous female mice, but not in hemizygous male or homozygous female mice. A cross between a male chimeric founder (100% chimerism) and wild-type (wt) C57BL/6 mice resulted in offspring (F1 generation). The founders were bred with wt C57Bl/6 to produce heterozygous female mice (F1 generation), which were back crossed with wt C57BL/6 males to obtain hemizygous males (F2 generation). Successive back-crosses were performed to generate transgenic mice with a homogeneous C57BL/6 genetic background. **(B)** The screening of offspring was performed by PCR, using a set of primers spanning the nephrin promoter and human c-mip (PCR1 product: 817 bp) and another set of primers specific for mouse HPRT (PCR2 product: 300 bp). The reconstituted HPRT gene was not amplified in homozygous female ($Tg^{+/+}$) or hemizygous male [Tg(+)] transgenic mice.

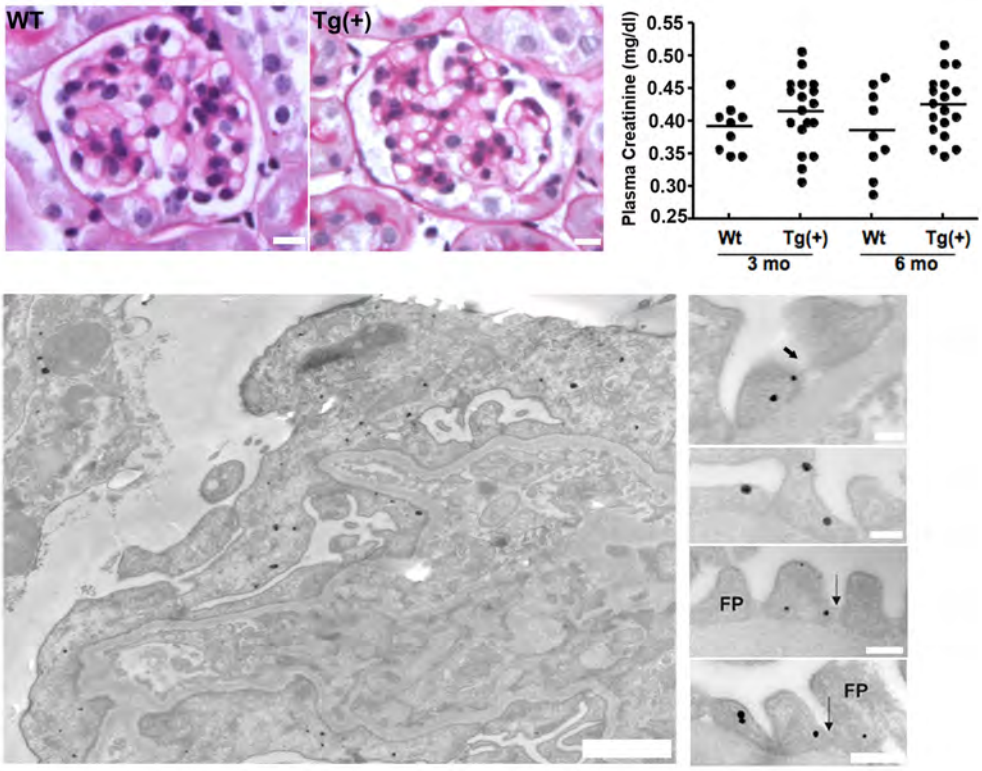

Figure S4. PAS staining of kidney sections from 8 week-old wt and proteinuric Tg(+) mice. Glomeruli and tubules of Tg(+) mice appear normal without inflammatory injury or cell proliferation. Tg(+) mice did not show changes in plasma creatinine. Each closed circle represents the value from an individual mouse. Immunogold labeling showing c-mip localization in podocyte foot processes (FP). c-mip is detected in close proximity to the slit diaphragm (arrows). Scale bars, left, 0.5 µM; right, 0.1 µM.

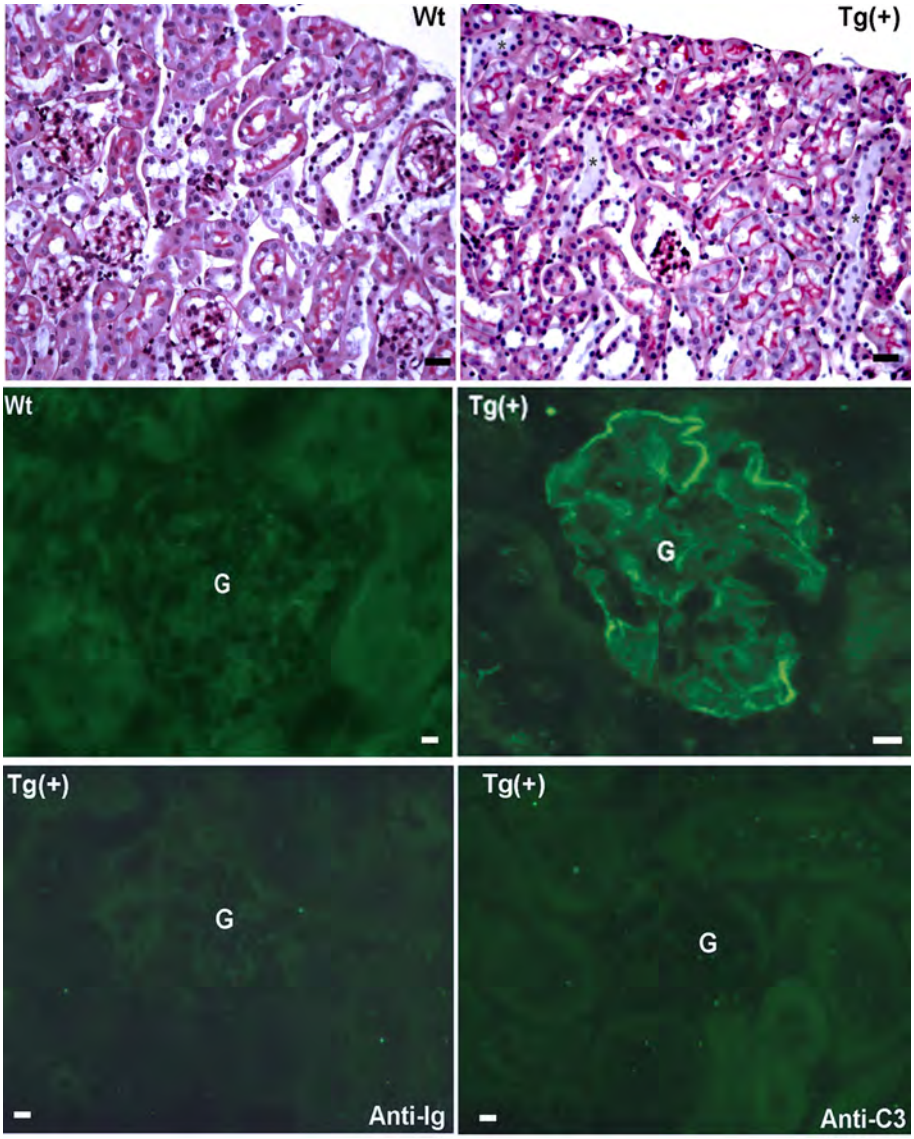
Wt
Tg(+)
Wt
G
Tg(+)
G
Tg(+)
G
Anti-Ig
Tg(+)
G
Anti-C3

Figure S5. Morphological characterization of c-mip transgenic mice. Upper panel, Hematoxylin and eosin staining of kidney sections from 8 week-old wt and proteinuric Tg(+) mice. Some tubules of Tg(+), but not wild-type, mice are filled with proteins (asterisks). Middle panel, Immunofluorescence analysis on kidney sections. Expression of c-mip is detected in glomeruli (G) of Tg(+) mice but not in wild-type mice. Lower panel, Immunofluorescence analysis on kidney sections using anti-mouse immunoglobulin and anti-complement 3. No staining has been observed. Scale bars, upper panel, 50 μM; middle and lower panels, 10 μM.

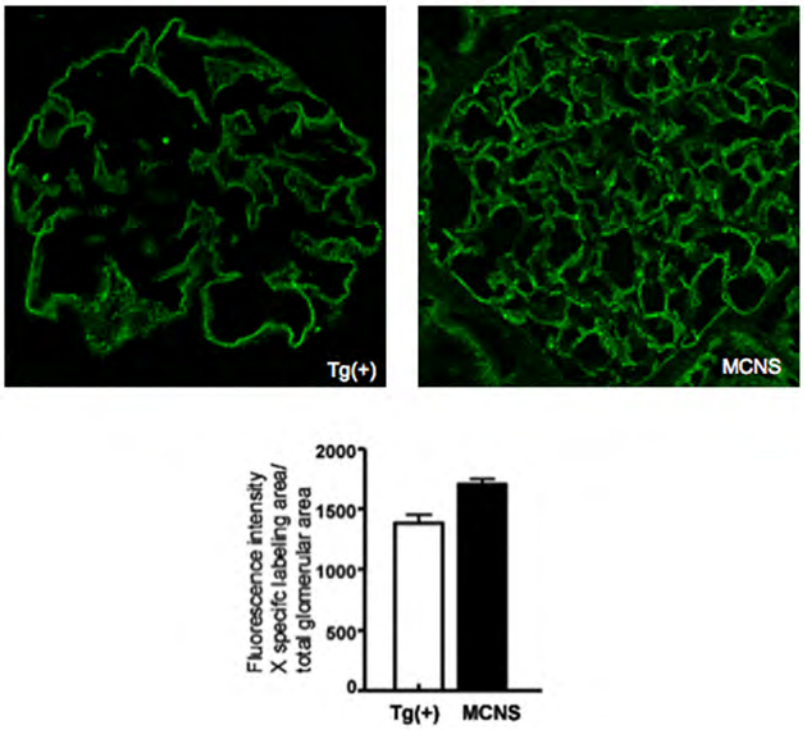

Figure S6. Quantitation of confocal microscopy analysis of c-mip abundance in glomeruli of MCNS kidney biopsies and renal tissue of Tg(+) mice. The abundance of c-mip was assessed by quantifying the specific glomerular fluorescence intensity (lining the capillary loops) in 3-D stacks of images taken by confocal microscopy and normalized to total glomerular area. Results are presented in table S2. Data represent the means ± SEM

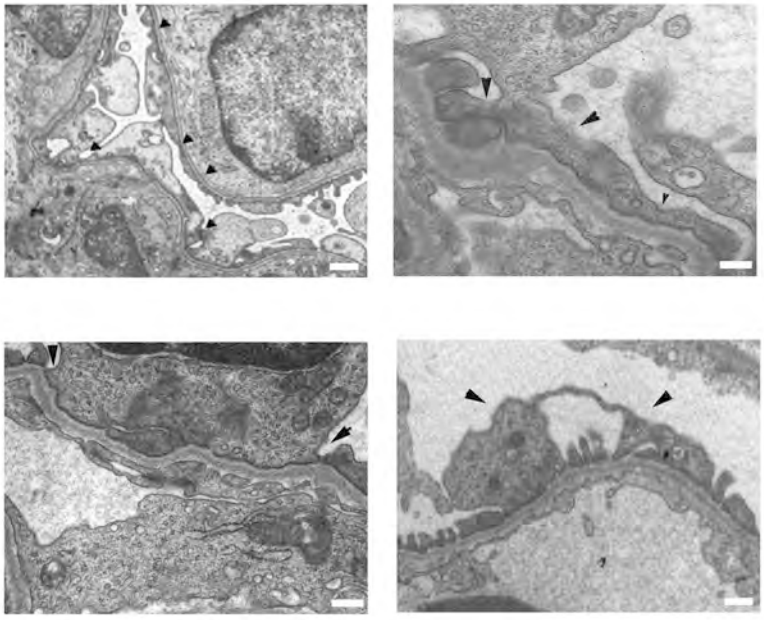

Figure S7. Ultrastructural analysis of podocytes from 5 day-old newborn transgenic mice.Magnification micrograph from podocyte shows area of foot process effacement and anormalfoot process development. Scale bars, 0.1 μM.

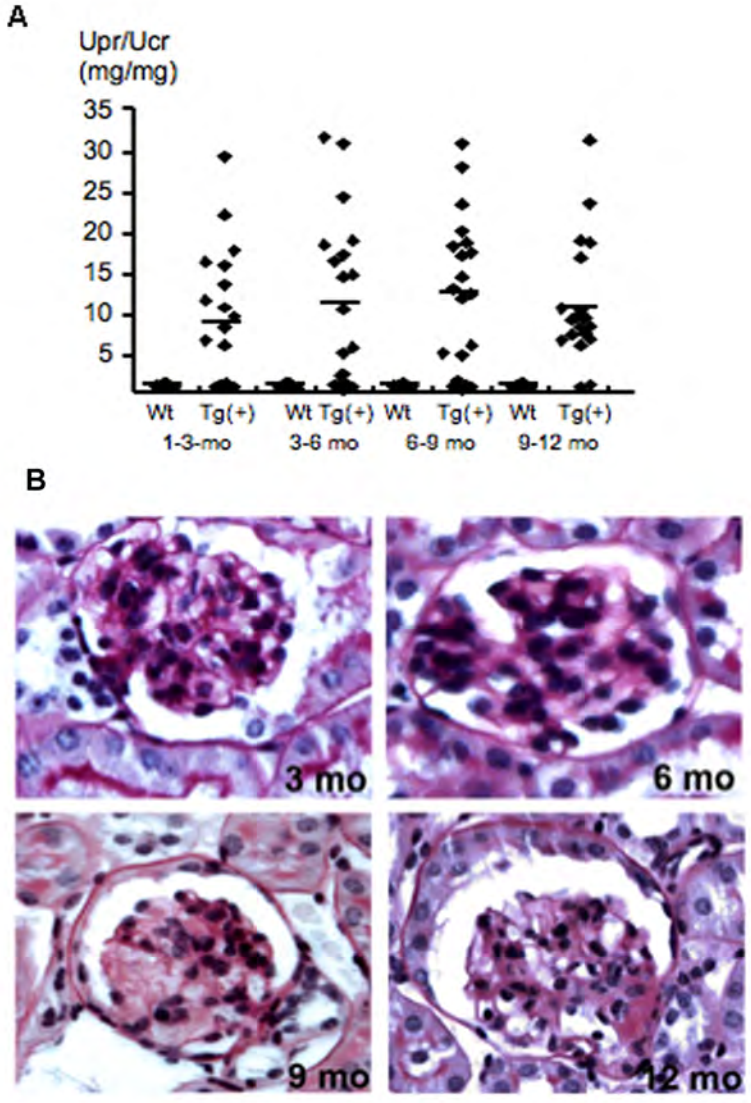

Figure S8. Course of glomerular disease in Tg(+) mice. (A) Proteinuria (proteinuria/creatinine ratio, Upr/Ucr) was measured in Tg(+) and wild-type mice at different ages (1 month to one year). (B) Histopathological analysis. Kidney sections from nephrotic Tg(+) mice of different ages were stained with PAS and graded by light microscopy in a blind fashion for proliferation and chronicity indices. Each closed circle represents histological evaluation from a single mouse. Focal mesangial hypercellularity was observed from 3-4 months, whereas few FSGS-like lesions and significant mesangial matrix expansion appeared later.

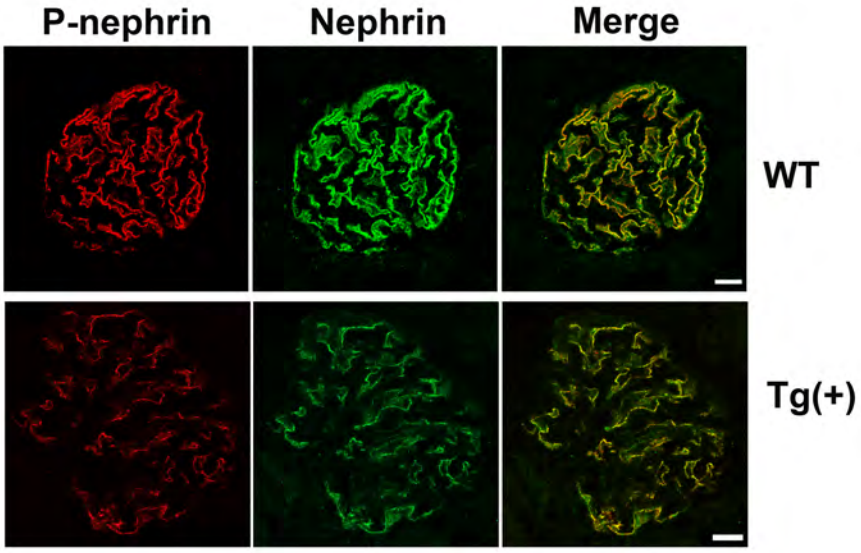

Figure S9. Confocal microscopy analysis of the abundance of total and phosphorylated nephrin in kidney sections from 8 week-old wild type and Tg(+) mice. Total nephrin, green; phosphorylated nephrin, red. Nephrin was present in some capillary loop areas, but phosphonephrin was not as well visualized. Scale bars, 10 μM.

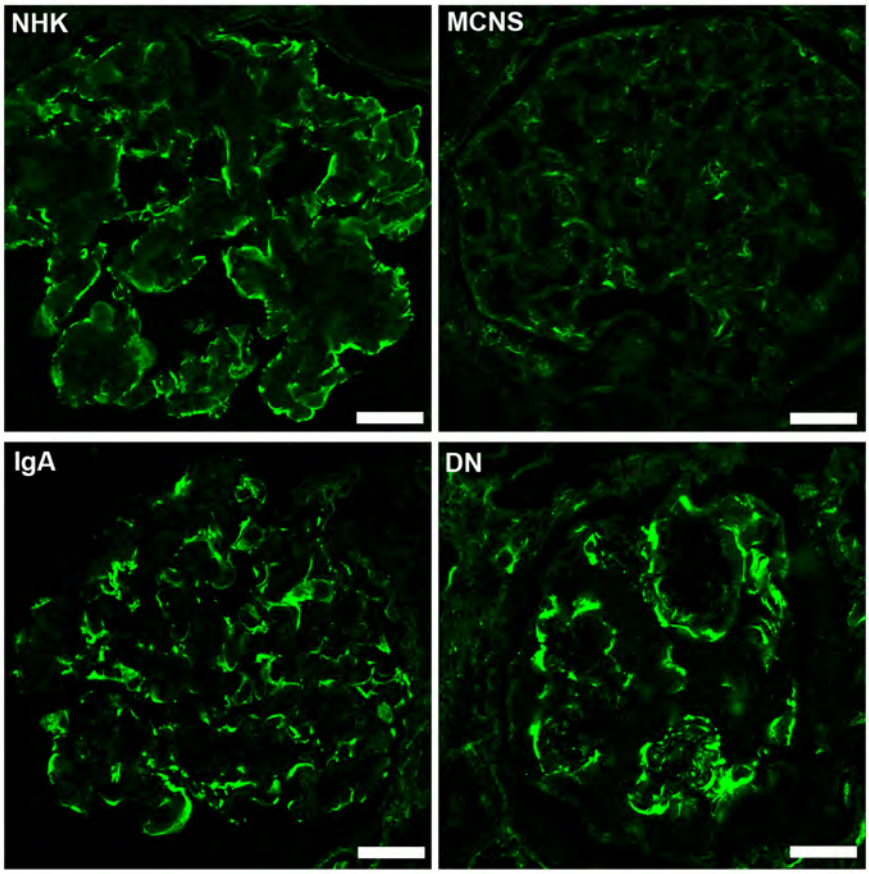

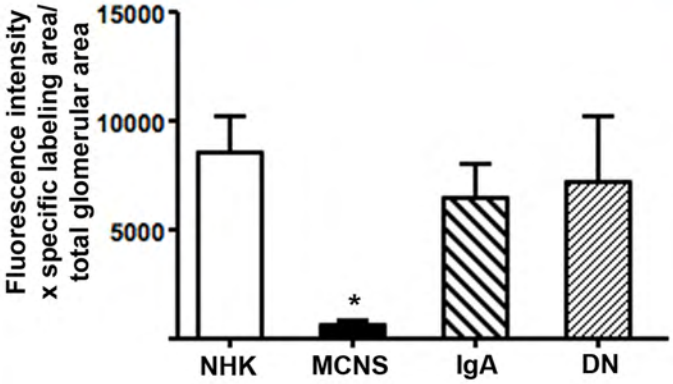

Figure S10. Quantitation of confocal microscopy analysis of phosphorylation of Ser473 in Akt in glomerular diseases. Representative immunofluorescence analysis of pSer473-Akt in glomeruli of normal human kidney (NHK, n=3), MCNS (n=5), IgA nephropathy (n=5) and diabetic nephropathy (DN, n=3). The relative abundance of pSer473-Akt was assessed by quantifying the specific glomerular fluorescence intensity (five to ten glomeruli by biopsy). The amount of pSer473-Akt is significantly reduced in MCNS, as compared with NHK, IgA or DN (p< 0, 05, Kruskal-Wallis test). Scale bars, 10 µM.

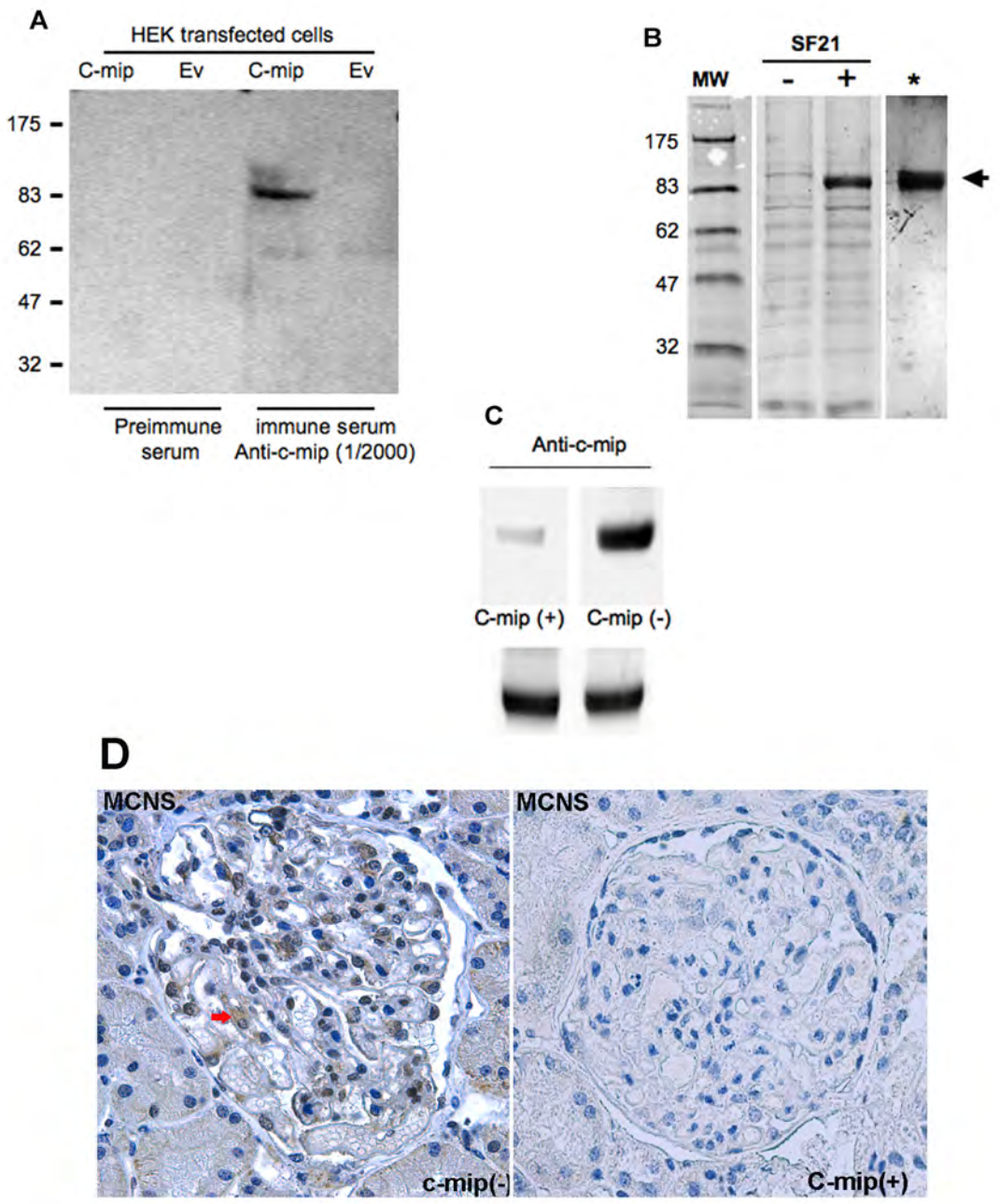

Figure S11. Specificity the anti-c-mip antibody. (A) Western blot of protein lysates from HEK 293 cells overexpressing c-mip or empty vector (Ev). The c-mip antibody recognized overexpressed c-mip. HEK 293 cells lack endogenous c-mip. (B) SDS-PAGE analysis of supernatants of baculovirus non-infected (-) or infected (+) Sf21 cells.The right lane(asterisk) shows the purification of c-mip from supernatants of baculovirus-infected sf21 cells by preparative SDS-PAGE and gel electroelution. (C) Western blot of c-mip without (lower panel) or after (upper panel) preadsorption with the recombinant c-mip protein purified from supernatants of baculovorus-infected Sf9 cells. The reactivity of anti-c-mip antibody was abolished after preadsorption. (D) Immunostaining of MCNS biopsy with anti-c-mip antibody before (-) and after (+) adsorption with c-mip protein.

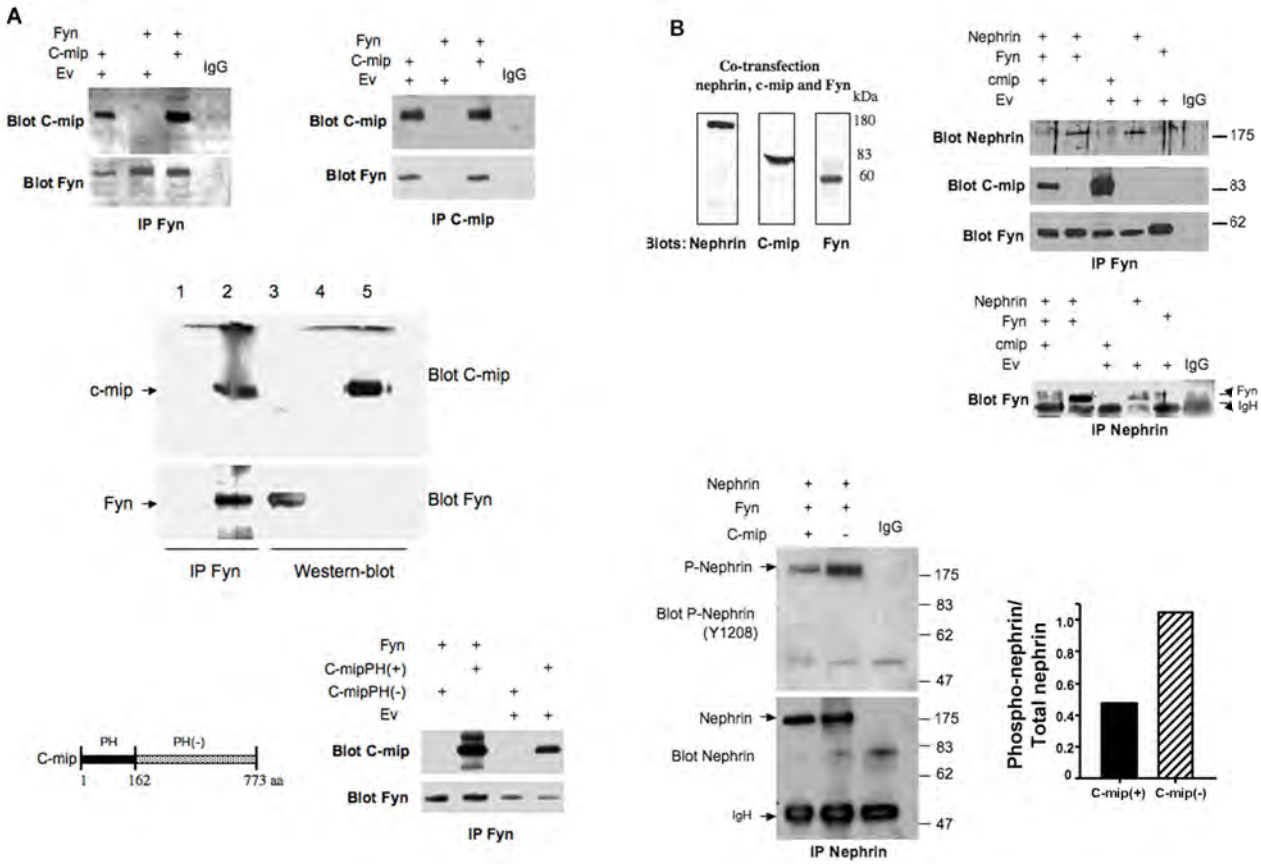
A
Fyn
C-mip
Ev
IgG
Blot C-mip
Blot Fyn
IP Fyn
IP C-mip
1 2 3 4 5
c-mip
Fyn
Blot C-mip
Blot Fyn
IP Fyn
Western-blot
C-mip
PH
PH(-)
1
162
773 aa
C-mipPH(+)
C-mipPH(-)
B
Co-transfection
nephrin, c-mip and Fyn
kDa
180
83
60
Blots: Nephrin C-mip Fyn
Nephrin
cmip
Blot Nephrin
IP Fyn
IP Nephrin
P-Nephrin
Blot P-Nephrin
(Y1208)
IgH
Phospho-nephrin/
Total nephrin
C-mip(+)
C-mip(-)

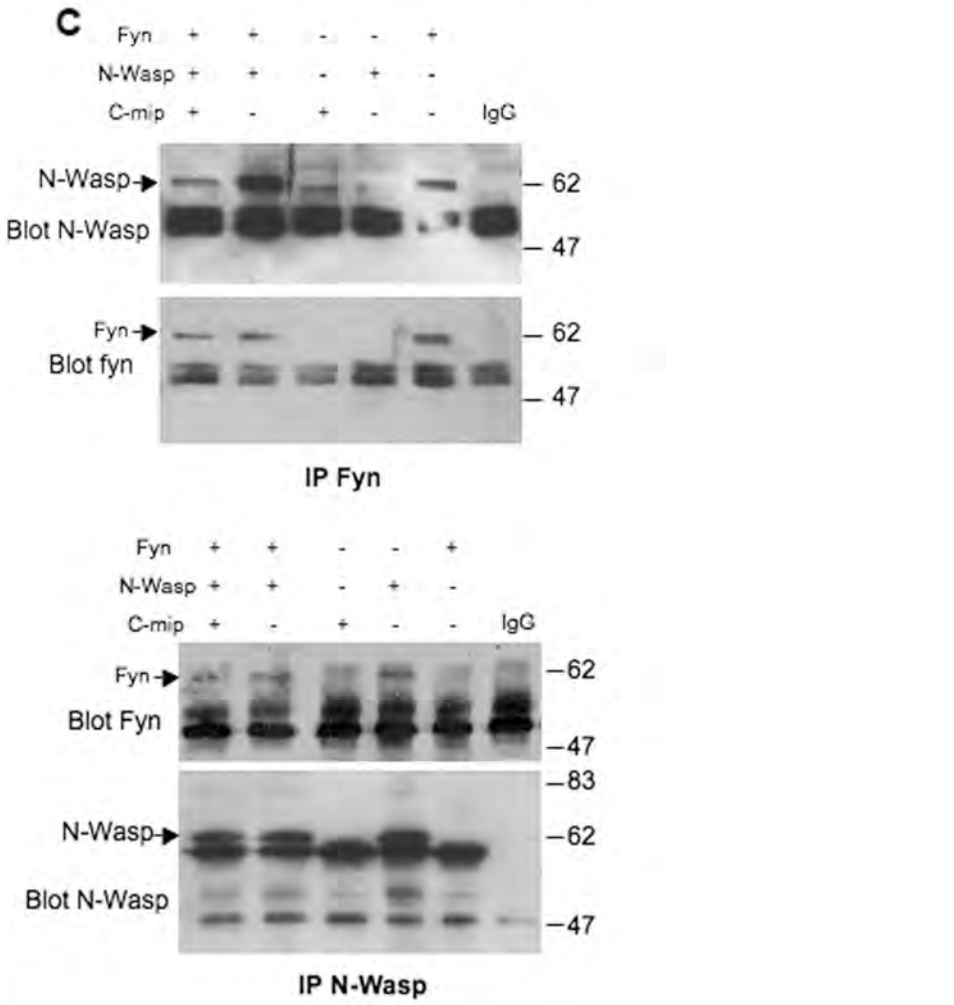
C
Fyn
N-Wasp
C-mip
IgG
N-Wasp
Blot N-Wasp
Fyn
Blot fyn
62
47
IP Fyn
Blot Fyn
83
IP N-Wasp

Figure S12. (**A)** c-mip is a partner of Fyn (upper panel). HEK 293 cells were cotransfected with c-mip and Fyn or empty vector (Ev). Protein lysates were immunoprecipitated with either anti-Fyn (left panel) or anti-c-mip (right panel) and eluates were probed with anti-c-mip or anti-Fyn antibody, respectively. c-mip interacts directly with Fyn (middle panel). The recombinant Fyn protein was incubated with the recombinant c-mip protein purified from supernatants of c-mip-infected Sf21 cells, followed by immunoprecipitation with anti-Fyn antibody (lane 2) or mouse IgG control (lane 1). The eluates were incubated with c-mip and Fyn. In parallel, Western blotting of recombinant Fyn (lane 3) and non-infected (lane 4) or c-mip-infected Sf21 cells (lane 5) are indicated; the lower panel shows the immunoprecipitation of Fyn from HEK 293 cells cotransfected with Fyn and truncated forms of c-mip consisting of a PH domain alone [PH(+)] or c-mip deleted of its PH domain [PH(-)].c-mip interacts with Fyn through its PH domain. **(B)** c-mip binds Fyn and prevents its interaction with nephrin, resulting in the inhibition of Fyn-mediated nephrin phosphorylation. HEK cells were cotransfected with c-mip, Fyn, nephrin and empty vector (Ev). Protein lysates were immunoprecipitated with anti-Fyn (upper panel) or anti-nephrin (lower panel) and eluates were blotted as indicated in the figure. c-mip inhibits the interaction of nephrin with Fyn (inputs are indicated in the left); lower panel, immunoblotting of phosphorylated nephrin in HEK cells cotransfected with Fyn and nephrin with or without c-mip. c-mip inhibits Fyn-mediated nephrin phosphorylation. Data represent one of two experiments. **(C) c**-mip binds Fyn and prevents its interaction with N-WASP. HEK 293 cells were cotransfected with Fyn and N-WASP with or without c-mip expression plasmids. Protein lysates were immunoprecipitated with either anti-Fyn (upper panel) or anti-N-WASP (lower panel) and eluates were probed with anti-N-WASP or anti-Fyn, respectively. The interaction of Fyn with N-WASP is inhibited in the presence of c-mip. The control consists of immunoprecipitation of protein extracts with rabbit IgG.

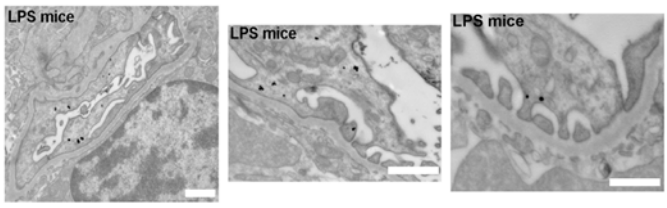

Figure S13. Immunogold labeling showing c-mip localization in primary and secondary podocyte foot processes (FP) in LPS–treated mice. Scale bars, 0.5 μM.

Patients	Mean age in years	Proteinuria g/24 hours	Hematuria RBC/ml	Albuminemia g/l (range)	Serum creatinine µmol/l	Light microscopy	IF Ig/C deposits
Active MCNS (n=15)	23 (21-35)	9.5 (3.3-15.6)	$< 10^4$	15.3 (10-21)	104 (71-158)	Normal	Negative (13), IgM (2)
MCNS remission (n=5)	10 (7-13)	Negative	$< 10^3$	40 (37-43)	60	Normal	Negative
MN (n=12)	34 (27-49)	6 (4-9)	22,500 (10^4-4.10^4)	12.1 (9.7-14)	115 (86-150)	Diffuse glomerular capillary thickening with spikes	IgG/C3
IgA nephropathy (n=5)	31 (25-42)	5 (3-6.7)	116,000 (6.10^4-20.10^4)	34.9 (32.8-38)	77.6 (65-85)	Mesangial cell proliferation and matrix increase	IgA/C3
Diabetic nephropathy (n=3)	47 (42-55)	9.5 (6-14)	$\leq 10^4$	23 (17.9-28)	197.5 (175-220)	Nodular sclerosis Diffuse mesangial expansion	Negative
FSGS (n=10)	38 (31-54)	5 (3.1-9.2)	4.10^4 (10^4-$2.5.10^5$)	21 (11-36)	120 (78-170)	Segmental sclerosis and adhesion; glomerular hyaline foci; discrete hypercellularity	IgM (3) IgM/C3 ; C1q (1) IgM/C3 (6)
HIVAN (n=3)	28 (21-35)	8 (7-9)		16 (14-17)	220 (180-280)	Collapsing glomerulopathy	IgG/IgM/C3

Table S1. Characteristics of the patients at the time of biopsy

Abbreviations: MCNS, minimal change nephrotic syndrome; MN, membranous nephropathy; MGN, mesangial glomerulonephritis; FSGS, focal segmental glomerulosclerosis; IF, immunofluorescence

Kidney biopsy was performed in patients with MCNS remission in order to check whether the histological signs of ciclosporine toxicity were occured

Ranges are indicated in parentheses

	Fluorescence mean intensity	*Labeled glomerular area /total glomerular area*	*Standard deviation*	*Lower threshold*	*Upper threshold*	*Quantification Q= F X S*
Tg(+)1	2521.14	*0.623561*	*492.33*	*2000*	*4095*	*1572.08458*
Tg(+)2	*2393.25*	*0.560362*	*372.45*	*2000*	*4095*	*1341.08636*
Tg(+)3	*2342.42*	*0.505857*	*322.64*	*2000*	*4095*	*1184.92955*
Tg(+)4	*2504.49*	*0.658838*	558.08	*2000*	*4095*	*1650.05318*
Tg(+)5	*2462.43*	*0.559456*	*436.55*	*2000*	*4095*	*1377.62124*
Tg(+)6	*2341.31*	*0.734343*	*570.82*	*2000*	*4095*	*1719.32461*
MCNS-1	*2554.91*	*0.720426*	*541.71*	*2000*	*4095*	*1840.62359*
MCNS-2	*2698.39*	*0.635036*	*632.02*	*2000*	*4095*	*1713.57479*
MCNS-3	*2676.55*	*0.692628*	*598.93*	*2000*	*4095*	*1853.85347*
MCNS-4	*2468.79*	*0.581149*	*468.35*	*2000*	*4095*	*1434.73484*
MCNS-5	*2640.85*	*0.746948*	*592.70*	*2000*	*4095*	*1972.57763*

Table S2. Quantification of c-mip abundance in glomeruli of MCNS kidney biopsies and Tg(+) mice. Ten entire glomeruli by tissue section were analyzed by confocal microscopy. 3-D image stacks were processed and quantitative analyses were performed using Image J software. The mean data for each kidney biopsy or Tg(+) kidney section are summarized.

Proteinuria / mice	negative	traces	+ (30 mg/dl)	++ (100 mg/dl)	total number
Wild-type-21d	22	19			41
F7-5d	4	4	16	3	27
F7-10d	4	30	24	4	62
F7-21d ($Tg^{+/+}$) females	2	4	6	5	17
F7-21d Tg(+) males	1	3	8	7	19

Table S3. Semi-quantitative measurement of urinary protein concentration in newborn transgenic and wild-type mice. F7 generation transgenic mice between 5 and 21 postnatal days (d) of age were analyzed. Forty-one 3 week-old wild–type mice were analyzed.

Primers	Sequence	Accession number	Expected size	Ann Temp (°C)	PCR cycles
Riboprobe 1	Forward: TGGAAAACTCAGTCTCCTACAGCGC Reverse : CGTTCCGGATTTCCTTCAGGCT	AK096598	759	60	32
Human Cmip Full length	Forward GGGGACAAGTTTGTACAAAAAAGCAGGCTTCG AAGGAGATAGAACCATGGATGTGACCAGCAGC TCGGGCGGCGGCGGCGAC Reverse GGGGACCACTTTGTACAAGAAAGCTGGGTC CCAGGCTTCGGTGTAGCGGACGTCCACTTCCT	AK096598	2319	60	32
Tansgene	Forward (nephrrin promoter): CGTGAACCTGCTGGACTTAGAGCAGCCG Reverse (cmip): CACTGGTCTCGCAGGTAGCTATTGGCAG		807	60	32
Mouse primers					
	c-mip Forward: CTGAACGAGCTCAACGCAGGCAT Reverse: GACAATGTGGCTTCCTGAGACACCA	XM_924798.	284	64	35
	HPRT Forward: GAGGGAGAAAAATGCGGAGTG Reverse: CTCCGGAAAGCAGTGAGGTAAG	NM_013556	300	62	34
	18S Forward: GTAACCCGTTGAACCCCATT Reverse: CCATCCAATCGGTAGTAGCG	NR_003278.	150	55	32
	N-WASP Forward: GGGGACAAGTTTGTACAAAAAAGCAGGCTTCGAAG GAGATAGAACCATGAGCTCGGGCCAGCAGCCCCCGC Reverse: GGGGACCACTTTGTACAAGAAAGCTGGGTCGT CTTCCCACTCATCATCATCCTC	AJ318416	1506	62	32

Table S4. Sequence of primers and PCR conditions.

The underlined sequences correspond to attB-sites used to incorporate the PCR product into the gateway plasmids.